NASA TR R-145

NATIONAL AERONAUTICS AND SPACE ADMINISTRATION

TECHNICAL REPORT
R-145

AN INVESTIGATION OF THE VIBRATION CHARACTERISTICS OF PRESSURIZED THIN-WALLED CIRCULAR CYLINDERS PARTLY FILLED WITH LIQUID

By JOHN S. MIXSON and ROBERT W. HERR

1962

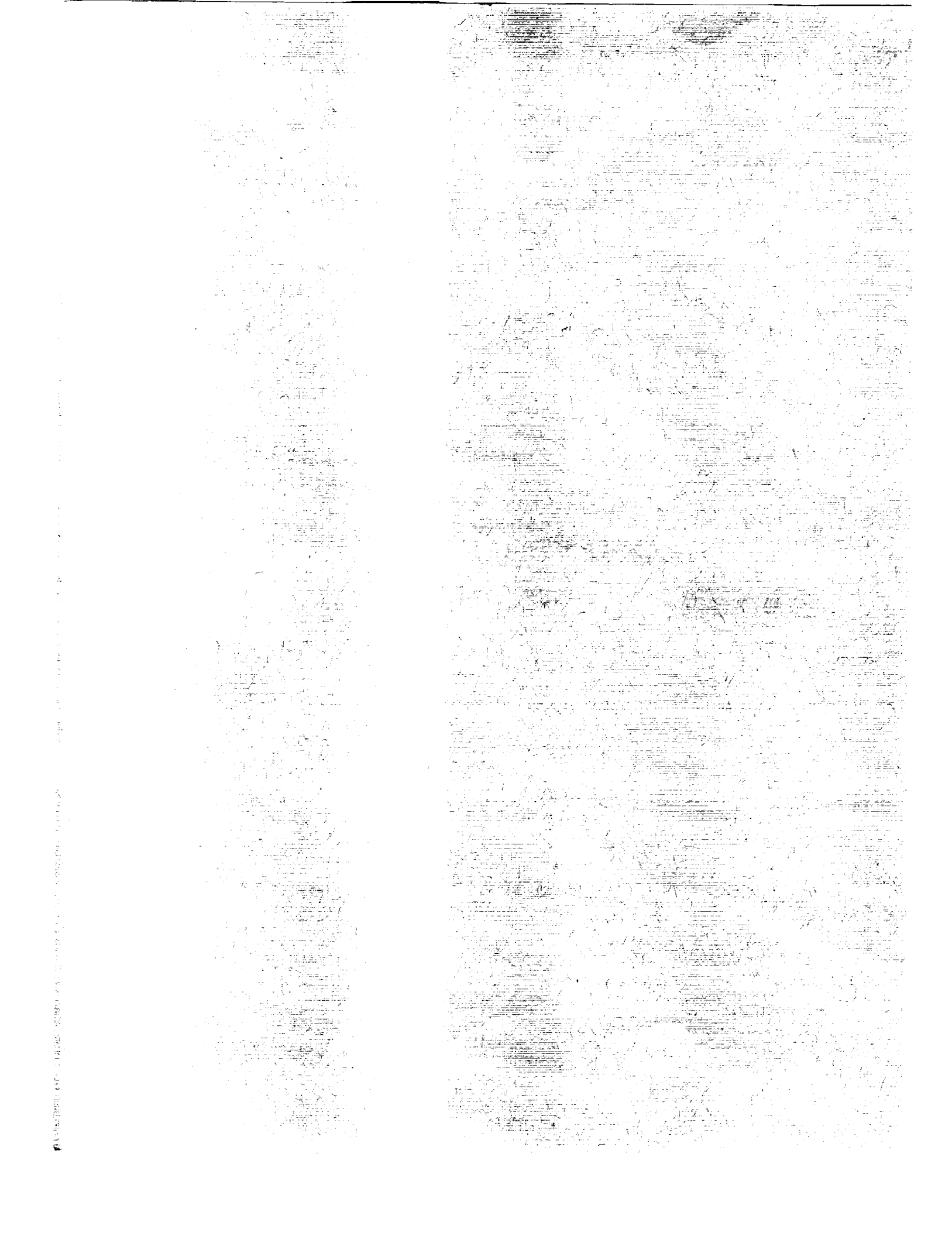

ERRATA

NASA Technical Report R-145

AN INVESTIGATION OF THE VIBRATION CHARACTERISTICS OF PRESSURIZED THIN-WALLED CIRCULAR CYLINDERS PARTLY FILLED WITH LIQUID

By John S. Mixson and Robert W. Herr
1962

Page 4: In the first line below equations (3), the word "strains" should be "stresses."

Page 7, equation (20): On the right-hand side of this equation, the symbol $W_s(t)$ following the summation sign should be $\dot{W}_s(t)$.

Page 8, equation (29): On the right-hand side of this equation, the cosine term should have a rule inserted between the numerator and denominator, thus,

$$\cos \frac{2\lambda_s b}{a}$$

Page 36, equation (A5): In the first term within the brackets, the symbol $W_s(t)^2$ should be $\dot{W}_s(t)^2$.

Issued 2-14-64

NASA-Langley, 1964

TECHNICAL REPORT R-145

AN INVESTIGATION OF THE VIBRATION CHARACTERISTICS OF PRESSURIZED THIN-WALLED CIRCULAR CYLINDERS PARTLY FILLED WITH LIQUID

By JOHN S. MIXSON and ROBERT W. HERR

Langley Research Center
Langley Station, Hampton, Va.

TECHNICAL REPORT R-145

AN INVESTIGATION OF THE VIBRATION CHARACTERISTICS OF PRESSURIZED THIN-WALLED CIRCULAR CYLINDERS PARTLY FILLED WITH LIQUID

By John S. Mixson[1] and Robert W. Herr

SUMMARY

Equations are derived for the calculation of the natural frequencies of shell vibration of pressurized, thin-walled, circular cylinders which are empty, partly filled, or full of liquid. In this type of vibration the axis of the cylinder is undeformed and the cross-section shape deforms during the vibration. The derivation follows a Rayleigh-Lagrange procedure, in which expressions for kinetic and potential energy are developed in terms of the displacements of the cylinder, the displacement shapes are assumed, and Lagrange's equations are applied to give a set of linear simultaneous equations of motion which, upon substitution of simple harmonic motion, yield a frequency determinant.

Also presented are experimentally determined natural frequencies and mode shapes of two cylinders having ratios of radius to thickness of 937 and 3,000. Natural frequencies of both cylinders were determined for internal pressures up to 8 psig and ratios of liquid depth to cylinder length from 0 to 1.47.

Comparisons between the theoretical and experimental frequencies indicate that the equations derived herein are adequate for prediction of the experimental frequencies of the cylinders tested. Both calculated and experimental results show that when the cylinders are greater than half full, their frequencies are less than half of the corresponding frequencies of the cylinders when empty. Also, the damping of a water-filled cylinder was found experimentally to be less than the damping of the empty cylinder.

INTRODUCTION

Thin-walled, unstiffened, circular cylinders are presently being used extensively as combination fuel tanks and primary structure in the design of liquid-fueled rockets. The need for structural efficiency, which dictates that the structure be as light as possible, combined with the presence of high-energy vibration sources, such as the rocket engines and boundary layer, has emphasized the importance of dynamic loading problems for these thin-walled tanks. Of prime importance with respect to the dynamic loading problems are the natural modes and associated natural frequencies of vibration, which for a booster vehicle include beam vibrations, shell vibrations, and fuel sloshing, each of which can possibly couple with the others or with the control system. In this report the vibrations considered are the shell vibrations (sometimes referred to as "breathing," "wall," or "lobar" vibrations), wherein the axis of the cylinder remains undeformed and the elements of the wall perform harmonic motions in the axial, radial, and circumferential directions.

Shell vibration frequencies of thin-walled cylinders have been calculated by many authors, among the first of which were Lord Rayleigh (ref. 1) and A. E. H. Love (ref. 2). Both Rayleigh and Love presented frequency equations for shells with either infinitely thin walls or an inelastic middle surface (an imaginary surface located at midthickness of the shell wall). Baron and Bleich (ref. 3) extended Rayleigh's work to include both

[1] Information presented herein is being offered by Mr. John S. Mixson in partial fulfillment of the requirements for the degree of Master of Applied Mechanics, University of Virginia, Charlottesville, Virginia.

finite wall thickness and middle surface elasticity in the frequency equation. Reissner (ref. 4) derived a frequency equation including the effects of finite wall thickness, middle surface elasticity, and internal pressure. Berry and Reissner (ref. 5) extended this work to include, in addition, the effect of an internal compressible fluid. Baron and Bleich (ref. 6) investigated shell vibrations of unpressurized cylinders partly filled with liquid with the ends freely supported at the bottom and free at the top. Comparisons between calculated and experimentally determined frequencies were presented by Arnold and Warburton (refs. 7 and 8), who investigated vibrations of unpressurized cylinders with fixed or freely supported ends, and by Fung, Sechler, and Kaplan (ref. 9), who investigated vibrations of internally pressurized cylinders. These comparisons showed good agreement between the calculated and experimentally determined frequencies.

In this paper, a frequency equation is derived for shell vibrations of thin-walled circular cylinders partly filled with liquid, containing internal pressure, and having freely supported ends. An experimental program to determine the natural frequencies of two thin-walled cylinders having a variety of combinations of internal pressure and water level was also conducted for comparisons with the theory. The derivation of the frequency equation is presented first, then the experimental program, and finally, comparisons of the theory with experiment.

SYMBOLS

a	mean radius of cylinder
b	depth of liquid
$B_s(t), C_j(t), D_j(t)$	time-dependent coefficients appearing in equation (18)
E	Young's modulus
f	frequency of natural vibration, $\omega/2\pi$, cps
$f_n(\lambda_s)$	virtual mass factor, $\frac{I_n(\lambda_s)}{\lambda_s I_n'(\lambda_s)}$
g	acceleration of gravity
g_1	damping factor, defined by equation (56)
G	shear modulus, $\frac{E}{2(1+\mu)}$
h	wall thickness
I_n	modified Bessel function of first kind of order n
I_n'	derivative of I_n with respect to its argument
J_n	Bessel function of first kind of order n
i, j, k, s	summation indices
$K_1(s, k), K_2(s)$	expressions defined by equations (28) and (29)
L	cylinder length
m	number of axial half-waves
$m_{v1}(s), m_{v2}(s,k)$	liquid virtual mass coefficient, defined by equations (31) and (32) or (33) and (34)
n	number of circumferential waves
$\mathbf{n}$	unit vector normal to liquid boundary
$N+1$	number of terms in series expansion of displacements
p	internal pressure
$q(s), q_1(s, k)$	expressions defined by equations (41) and (42)
r	radial coordinate
t	time
T	kinetic energy
u, v, w	displacements of a point on middle surface in the axial, circumferential, and radial directions, respectively
$U_s(t), V_s(t), W_s(t)$	amplitude and time-varying part of displacements
V	potential energy
v_r, v_φ, v_x	velocities of the liquid in radial, circumferential, and axial directions, respectively
x_1, x_2	height of circumferential node line above cylinder bottom (subscripts 1 and 2 denote first and second node lines, respectively)
x, y, z	coordinates with origin on surface at the base of the cylinder (fig. 2)
α_{nj}	roots of the equation $J_n'\left(\frac{\alpha_{nj}r}{a}\right)\Big\vert_{r=a}=0$
β	thickness-radius parameter, $\frac{h^2}{12a^2}$
γ	shear strain in middle surface
γ_{xy}	shear strain of element
Δ	frequency parameter, $\frac{(1-\mu^2)\rho_c a^2\omega^2}{Eg}$
ϵ_x, ϵ_y	direct strains of cylinder skin element

ϵ_1, ϵ_2	direct strains in middle surface
κ_1, κ_2, κ_{12}	changes of curvature and twist in middle surface associated with displacement w
λ_s	axial wavelength parameter, $\frac{(m+s)\pi a}{L}$
μ	Poisson's ratio
ν	number of cycles of vibration used to determine damping
ρ	weight density
σ_x, σ_y	direct stresses
τ_{xy}	shear stress
φ	angular coordinate
Φ	velocity potential of liquid
ω	circular frequency of natural vibration

Subscripts:

f	fluid (liquid and gas)
l	liquid
c	shell

A dot over a quantity indicates differentiation with respect to time.

THEORY

When a thin-walled cylinder vibrates in a shell mode the axis remains undeformed and the cylinder walls deform in a wave pattern as illustrated in figure 1. A number of stationary waves are formed in cross sections normal to the axis, as illustrated by the circumferential wave forms, and in cross sections containing the axis, as illustrated by the axial wave forms. Node lines are defined as in references 7 and 8 by the positions of zero radial deflection (tangential deflection is not necessarily zero at these positions) and typical node-line arrangements are shown in figure 1(b). It has been shown (ref. 7) that for each combination of m (the number of axial half-waves) and n (the number of circumferential waves), there exist three distinct modes of motion and associated frequencies. In the mode associated with the lowest frequency the motion of an element of the shell is primarily radial. The frequencies associated with the other two modes are large compared with the radial mode frequency, and the primary motion of a shell element in these two modes is tangent to the middle surface, either axial or circumferential. In this analysis only the radial mode is to be considered; therefore, a mode is

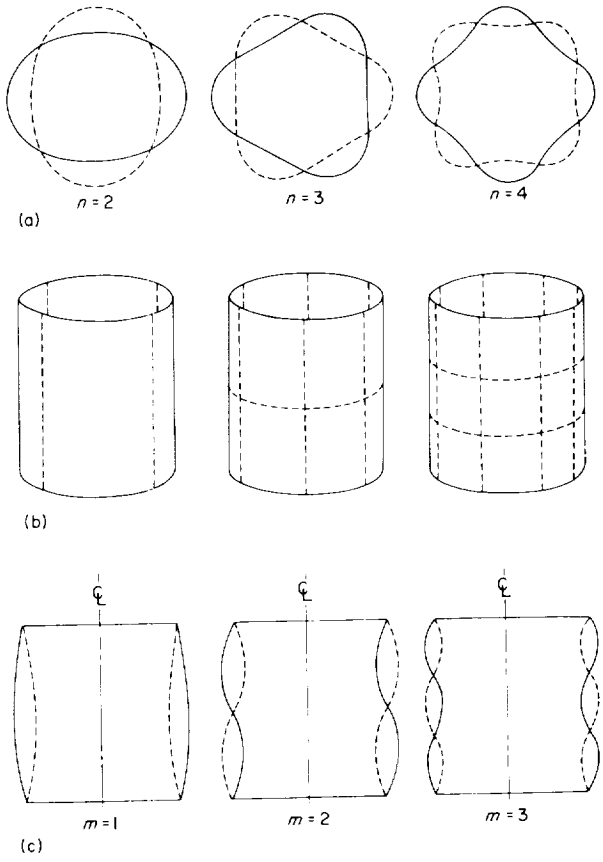

(a) Cross sections depicting circumferential wave forms.
(b) Node-line patterns.
(c) Cross sections depicting longitudinal wave forms.

FIGURE 1.—Typical deflection patterns of radial shell vibrations of thin-walled cylinders.

defined by the values of m and n. The frequencies of the tangential modes are prevented from appearing in the equations derived herein by neglecting the contribution to the kinetic energy of the tangential motions, both axial and circumferential.

A sketch of a cylinder with the coordinate system used in this analysis, together with an element of the shell, is shown in figure 2. The axis of the cylinder is vertical so that the liquid depth b is measured along the length L. The axial, circumferential, and radial displacements of a point on the middle surface u, v, and w are positive along the x-, y-, and z-axis, respectively, as shown in this figure.

DERIVATION OF POTENTIAL ENERGY

The potential energy of vibration of a thin-walled cylinder containing internal pressure can

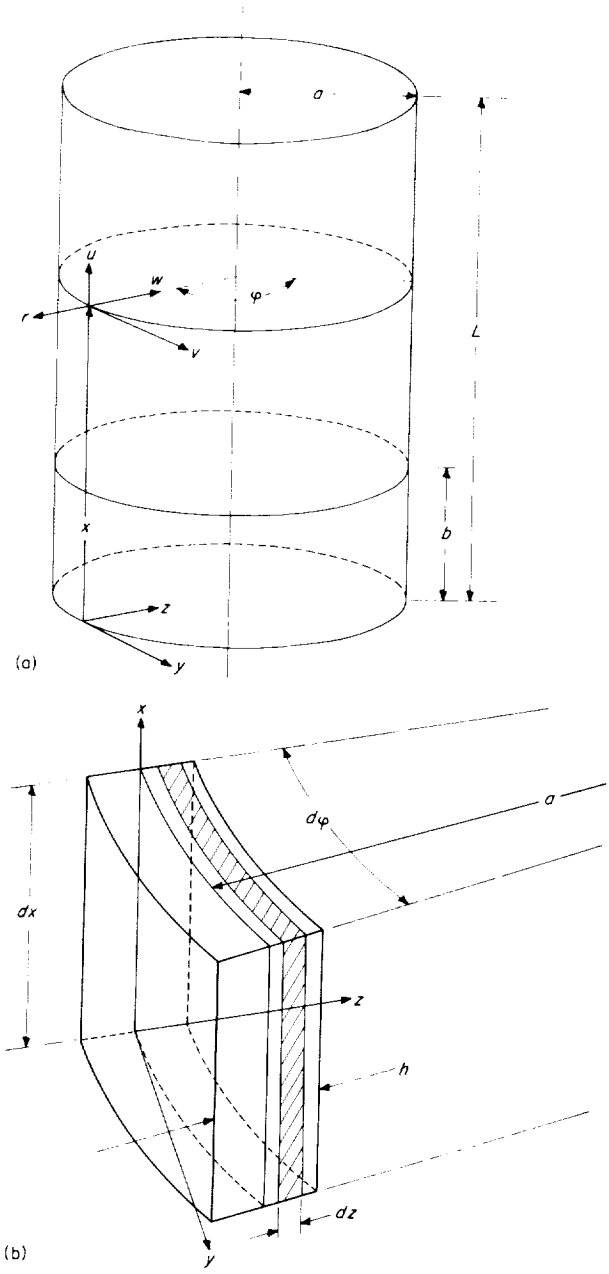

(a) Cylinder.
(b) Element.

FIGURE 2. - Sketch of cylinder showing coordinate system and a typical element of a thin cylindrical shell.

be written as:

$$V=\int_{-h/2}^{h/2}\int_0^{2\pi}\int_0^L \frac{1}{2}(\sigma_{x,c}\epsilon_x+\sigma_{y,c}\epsilon_y+\tau_{xy,c}\gamma_{xy})a\,dx\,d\varphi\,dz + \int_{-h/2}^{h/2}\int_0^{2\pi}\int_0^L (\sigma_{x,f}\epsilon_x+\sigma_{y,f}\epsilon_y+\tau_{xy,f}\gamma_{xy})a\,dx\,d\varphi\,dz \quad (1)$$

The stresses introduced in the first term on the right of this equation are associated with the elastic vibratory deflections of the cylinder as indicated by the subscript c, whereas those introduced in the second term are due to the internal fluid pressure, as indicated by the subscript f. This expression for strain energy neglects any contribution of stresses acting on the element in the direction perpendicular to the middle surface. The internal pressure and liquid stresses are assumed to be independent of the strains in the tank wall; and from Hooke's law, the shell-elasticity stresses are related to the strains by the expressions:

$$\left.\begin{aligned}\sigma_{x,c}&=\frac{E}{1-\mu^2}(\epsilon_x+\mu\epsilon_y)\\ \sigma_{y,c}&=\frac{E}{1-\mu^2}(\epsilon_y+\mu\epsilon_x)\\ \tau_{xy,c}&=\frac{E}{2(1+\mu)}\gamma_{xy}\end{aligned}\right\} \quad (2)$$

The strains ϵ_x, ϵ_y, and γ_{xy} in the element at a distance z from the middle surface of the shell are related to the middle-surface strains ϵ_1, ϵ_2, and γ and to the changes of curvature and twist κ_1, κ_2, and κ_{12} by the expressions (ref. 2, p. 529, for example):

$$\left.\begin{aligned}\epsilon_x&=\epsilon_1-z\kappa_1\\ \epsilon_y&=\epsilon_2-z\kappa_2\\ \gamma_{xy}&=\gamma-2z\kappa_{12}\end{aligned}\right\} \quad (3)$$

With the assumption that the pressure strains $\sigma_{x,f}$, $\sigma_{y,f}$, and $\tau_{xy,f}$ are constant across the thickness of the shell, equations (2) and (3) can now be substituted into equation (1) and the right-hand side integrated over the thickness of the shell to yield:

$$V=\frac{Eh}{2(1-\mu^2)}\int_0^{2\pi}\int_0^L\left(\epsilon_1^2+\epsilon_2^2+2\mu\epsilon_1\epsilon_2+\frac{1-\mu}{2}\gamma^2\right)a\,dx\,d\varphi + \frac{Eh^3}{24(1-\mu^2)}\int_0^{2\pi}\int_0^L [\kappa_1^2+\kappa_2^2+2\mu\kappa_1\kappa_2 + 2(1-\mu)\kappa_{12}^2]\,a\,dx\,d\varphi + h\int_0^{2\pi}\int_0^L(\sigma_{x,f}\epsilon_1+\sigma_{y,f}\epsilon_2 + \tau_{xy,f}\gamma)a\,dx\,d\varphi \quad (4)$$

The first, second, and third integral expressions in equation (4) represent the contributions to the strain energy of, respectively, the middle-surface elasticity, the bending of the finite-thickness shell

wall, and the internal pressure. The relations between the middle-surface strains ϵ_1, ϵ_2, and γ and the displacements of a point on the middle surface u, v, and w to be used are:

$$\left.\begin{aligned}\epsilon_1&=\frac{\partial u}{\partial x}+\frac{1}{2}\left(\frac{\partial w}{\partial x}\right)^2\\ \epsilon_2&=\frac{1}{a}\frac{\partial v}{\partial \varphi}-\frac{w}{a}+\frac{1}{2a^2}\left(\frac{\partial w}{\partial \varphi}\right)^2\\ \gamma&=\frac{1}{a}\frac{\partial u}{\partial \varphi}+\frac{\partial v}{\partial x}+\frac{1}{a}\frac{\partial w}{\partial x}\frac{\partial w}{\partial \varphi}\end{aligned}\right\} \tag{5}$$

In general, second-order terms involving u and v can also be included (for example, as in ref. 2, p. 60); however, with u and v assumed small in comparison with w, these terms are neglected. The expressions relating the changes of curvature and twist κ_1, κ_2, and κ_{12} to the displacements are:

$$\left.\begin{aligned}\kappa_1&=\frac{\partial^2 w}{\partial x^2}\\ \kappa_2&=\frac{1}{a^2}\frac{\partial^2 w}{\partial \varphi^2}\\ \kappa_{12}&=\frac{1}{a}\frac{\partial^2 w}{\partial x\partial \varphi}\end{aligned}\right\} \tag{6}$$

The expressions given by equations (6) neglect the effects of circumferential displacement on the changes of curvature and twist, a simplification suggested by shallow shell theory (ref. 10). When applied to cylindrical shell vibrations, shallow shell theory assumes that when the axial node lines are sufficiently close together, the portion of the shell between the node lines can be treated as a flat plate. Thus, as in flat-plate theory, the tangential displacements are assumed to have no effect on the changes of curvature, and equations (6) result. The stresses due to internal pressure and liquid are given by:

For $0<x<b$,

$$\left.\begin{aligned}\sigma_{x,f}&=\frac{pa}{2h}\\ \sigma_{y,f}&=\frac{pa}{h}+\frac{\rho_l a}{h}(b-x)\\ \tau_{xy,f}&=0\end{aligned}\right\} \tag{7a}$$

and for $b<x<L$,

$$\left.\begin{aligned}\sigma_{x,f}&=\frac{pa}{2h}\\ \sigma_{y,f}&=\frac{pa}{h}\\ \tau_{xy,f}&=0\end{aligned}\right\} \tag{7b}$$

Equations (5) to (7) are now substituted into equation (4) to give the following expression for potential energy in terms of the displacements:

$$\begin{aligned}V=&\frac{Eh}{2(1-\mu^2)}\int_0^{2\pi}\int_0^L\left[\left(\frac{\partial u}{\partial x}\right)^2+\frac{1}{a^2}\left(\frac{\partial v}{\partial \varphi}-w\right)^2+\frac{2\mu}{a}\frac{\partial u}{\partial x}\left(\frac{\partial v}{\partial \varphi}-w\right)+\frac{1-\mu}{2}\left(\frac{1}{a}\frac{\partial u}{\partial \varphi}+\frac{\partial v}{\partial x}\right)^2\right]a\,dx\,d\varphi\\ &+\frac{Eh^3}{24(1-\mu^2)}\int_0^{2\pi}\int_0^L\left[\left(\frac{\partial^2 w}{\partial x^2}\right)^2+\frac{1}{a^4}\left(\frac{\partial^2 w}{\partial \varphi^2}\right)^2+\frac{2\mu}{a^2}\frac{\partial^2 w}{\partial x^2}\frac{\partial^2 w}{\partial \varphi^2}+\frac{2(1-\mu)}{a^2}\left(\frac{\partial^2 w}{\partial x\partial \varphi}\right)^2\right]a\,dx\,d\varphi+pa\int_0^{2\pi}\int_0^L\left\{\frac{1}{2}\left[\frac{\partial u}{\partial x}\right.\right.\\ &\left.\left.+\frac{1}{2}\left(\frac{\partial w}{\partial x}\right)^2\right]+\frac{1}{a}\frac{\partial v}{\partial \varphi}-\frac{w}{a}+\frac{1}{2a^2}\left(\frac{\partial w}{\partial \varphi}\right)^2\right\}a\,dx\,d\varphi+\rho_l a\int_0^{2\pi}\int_0^b(b-x)\left[\frac{1}{a}\frac{\partial v}{\partial \varphi}-\frac{w}{a}+\frac{1}{2a^2}\left(\frac{\partial w}{\partial \varphi}\right)^2\right]a\,dx\,d\varphi\end{aligned} \tag{8}$$

It should be noted that the second-order terms of equations (5) have been omitted in the evaluation of the first integral expression of equation (4), since their contribution is small compared with the contribution of the first-order terms.

DERIVATION OF KINETIC ENERGY

When the kinetic energy of the tangential motion is neglected, the kinetic energy of the cylinder is given by

$$T_c=\frac{\rho_c h}{2g}\int_0^{2\pi}\int_0^L \dot{w}^2 a\,dx\,d\varphi \tag{9}$$

The kinetic energy of the incompressible, inviscid liquid is found from the relation

$$T_l=\frac{\rho_l}{2g}\int\int\Phi\frac{\partial\Phi}{\partial \mathbf{n}}\,dS \tag{10}$$

where the integral is taken over the entire surface boundary of the liquid, dS is an element of area of the liquid surface boundary, $\mathbf{n}$ is the outwardly directed unit vector normal to the liquid boundary, and Φ is a velocity potential function which satisfies

Laplace's equation

$$\nabla^2\Phi=\frac{\partial^2\Phi}{\partial r^2}+\frac{1}{r}\frac{\partial\Phi}{\partial r}+\frac{1}{r^2}\frac{\partial^2\Phi}{\partial\varphi^2}+\frac{\partial^2\Phi}{\partial x^2}=0 \tag{11}$$

and the following three boundary conditions:

(1) On the cylindrical surface $r=a$, the radial velocity of the fluid must be equal to the radial velocity of the shell; thus,

$$v_r|_{r=a}=\left.\frac{\partial\Phi}{\partial r}\right|_{r=a}=-\dot{w} \tag{12}$$

(2) On the bottom of the cylinder the axial fluid velocity must be zero; thus,

$$\left.\frac{\partial\Phi}{\partial x}\right|_{x=0}=0 \tag{13}$$

(3) On the free surface of the liquid the boundary condition is given by (ref. 11, ch. IX, article 227)

$$\left.\frac{\partial\Phi}{\partial t}\right|_{x=b}=g\eta+\frac{1}{2}(v_r^2+v_\varphi^2+v_x^2)+F(t) \tag{14}$$

where η is the displacement of the liquid surface from its undisturbed position and $F(t)$ is an arbitrary function of time. Since the velocities are small compared with the other terms, and since $F(t)$ may be absorbed into the potential Φ, this condition may be reduced to

$$\left.\frac{\partial\Phi}{\partial t}\right|_{x=b}=g\eta$$

As stated in reference 6, the contribution of the surface waves to the determination of the shell frequencies can be neglected because the liquid slosh frequencies are comparatively low. Therefore, for purposes of this paper, the effects of the surface waves are neglected ($g=0$) and the boundary condition on the free surface is reduced to

$$\left.\frac{\partial\Phi}{\partial t}\right|_{x=b}=0 \tag{15}$$

In view of these boundary conditions, the kinetic energy of the liquid (eq. (10)) can be written

$$T_l=\frac{\rho_l}{2g}\int_0^b\int_0^{2\pi}\left(\Phi\frac{\partial\Phi}{\partial r}\right)_{r=a}a\,d\varphi\,dx+\frac{\rho_l}{2g}\int_0^a\int_0^{2\pi}\left(\Phi\frac{\partial\Phi}{\partial x}\right)_{x=b}r\,d\varphi\,dr \tag{16}$$

The determination of Φ requires, from the first boundary condition, knowledge of the radial velocity of the shell and will therefore be completed after the assumed shell displacements are discussed.

CYLINDER DEFLECTION FUNCTIONS

If expressions for the displacements u, v, and w are now assumed, the strain and kinetic energies may be evaluated in terms of the amplitudes, and Lagrange's equation may be used to give a frequency equation. The expressions assumed for u, v, and w are:

$$\left.\begin{aligned}u&=\cos n\varphi\sum_{s=0}^{N}U_s(t)\cos\frac{\lambda_s x}{a}\\ v&=\sin n\varphi\sum_{s=0}^{N}V_s(t)\sin\frac{\lambda_s x}{a}\\ w&=\cos n\varphi\sum_{s=0}^{N}W_s(t)\sin\frac{\lambda_s x}{a}\end{aligned}\right\} \tag{17}$$

These deflection functions are the normal modes for the cylinder without liquid and will be coupled in the equations of motion by the hydrodynamic forces. Each term of the series satisfies end conditions known as freely supported, in which the cylinder ends are constrained to remain circular (radial deflection at the ends is zero) but no constraint is placed on the slope at the ends. This particular form of the sine and cosine series was chosen as a convenient way to obtain approximations to the higher axial modes without increasing the size of the frequency determinant. (It is shown subsequently that the frequency determinant is $3(N+1)$ terms by $3(N+1)$ terms.) For empty or liquid-filled cylinders it is usual to take only the first term of the expressions for u, v, and w; that is, $N=0$.

FLUID POTENTIAL FUNCTION

The kinetic energy of the liquid can now be evaluated from the displacements given by equation (17). The velocity potential satisfying Laplace's equation, $\nabla^2\Phi=0$, is

$$\Phi=\cos n\varphi\left\{\sum_{s=0}^{N}B_s(t)I_n\left(\frac{\lambda_s r}{a}\right)\sin\frac{\lambda_s x}{a}+\sum_{j=1}^{\infty}\left[C_j(t)\sinh\frac{\alpha_{nj}x}{a}+D_j(t)\cosh\frac{\alpha_{nj}x}{a}\right]J_n\left(\frac{\alpha_{nj}r}{a}\right)\right\} \tag{18}$$

where $B_s(t)$, $C_j(t)$, $D_j(t)$, and α_{nj} are to be determined from satisfaction of the boundary

conditions, and $I_n\left(\frac{\lambda_s r}{a}\right)$ and $J_n\left(\frac{\alpha_{nj} r}{a}\right)$ are Bessel functions of the first kind, modified and unmodified, respectively. This potential function can be obtained by discarding the terms which are inconsistent with the boundary conditions from the general solution of Laplace's equation in cylindrical coordinates. The first boundary condition (eq. (12)) will be satisfied if

$$\left.\frac{\partial J_n\left(\frac{\alpha_{nj} r}{a}\right)}{\partial r}\right|_{r=a}=0 \tag{19}$$

and

$$\sum_{s=0}^{N} B_s(t)\left.\frac{\partial I_n\left(\frac{\lambda_s r}{a}\right)}{\partial r}\right|_{r=a}\sin\frac{\lambda_s r}{a}=-\sum_{s=0}^{N} W_s(t)\sin\frac{\lambda_s r}{a} \tag{20}$$

Equation (19) is satisfied by the proper choice of α_{nj}, and equation (20) is satisfied with

$$B_s(t)=\frac{-2a\dot{W}_s(t)}{\lambda_s[I_{n-1}(\lambda_s)+I_{n+1}(\lambda_s)]} \tag{21}$$

Substitution of Φ (eq. (18)) into the second boundary condition (eq. (13)) yields the following equation for the determination of $C_j(t)$:

$$\sum_{s=0}^{N}\frac{\lambda_s}{a}B_s(t)I_n\left(\frac{\lambda_s r}{a}\right)+\sum_{j=1}^{\infty}\frac{\alpha_{nj}}{a}C_j(t)J_n\left(\frac{\alpha_{nj} r}{a}\right)=0 \tag{22}$$

For evaluation of $C_j(t)$, equation (22) is multiplied through by $rJ_n\left(\frac{\alpha_{nj} r}{a}\right)dr$ and integrated with respect to r from $r=0$ to $r=a$; use is then made of the orthogonality relation for Bessel functions

$$\left.\begin{aligned}\int_0^a J_n\left(\frac{\alpha_{ni} r}{a}\right)J_n\left(\frac{\alpha_{nj} r}{a}\right)r\,dr&=0 \qquad (i\neq j)\\ \int_0^a J_n\left(\frac{\alpha_{ni} r}{a}\right)J_n\left(\frac{\alpha_{nj} r}{a}\right)r\,dr&=\frac{a^2}{2}\left(1-\frac{n^2}{\alpha_{nj}^2}\right)J_n^2(\alpha_{nj}) \qquad (i=j)\end{aligned}\right\} \tag{23}$$

and the following integral

$$\int_0^a rI_n\left(\frac{\lambda_s r}{a}\right)J_n\left(\frac{\alpha_{nj} r}{a}\right)dr=\frac{a^2\lambda_s I_n'(\lambda_s)J_n(\alpha_{nj})}{(\alpha_{nj}^2+\lambda_s^2)}$$

This procedure yields the following expression for $C_j(t)$:

$$C_j(t)=-\frac{2a}{\alpha_{nj}\left(1-\frac{n^2}{\alpha_{nj}^2}\right)J_n(\alpha_{nj})}\sum_{s=0}^{N}\frac{\lambda_s\dot{W}_s(t)}{(\alpha_{nj}^2+\lambda_s^2)} \tag{24}$$

Upon substitution of Φ (eq. (18)) into the third boundary condition (eq. (15)), an expression for $\dot{D}_j(t)$ is obtained. Integration of this expression with respect to time yields the following expression for $D_j(t)$:

$$D_j(t)=-\frac{2a}{\alpha_{nj}\left(1-\frac{n^2}{\alpha_{nj}^2}\right)J_n(\alpha_{nj})}\sum_{s=0}^{N}\frac{\left(\alpha_{nj}\sin\frac{\lambda_s b}{a}-\lambda_s\sinh\frac{\alpha_{nj}b}{a}\right)\dot{W}_s(t)}{(\alpha_{nj}^2+\lambda_s^2)\cosh\frac{\alpha_{nj}b}{a}}+\text{Constant} \tag{25}$$

The constant is associated with the initial motion of the fluid and for purposes of this analysis can be neglected. The potential function Φ is now written in the form

$$\Phi=\cos n\varphi\sum_{s=0}^{N}\left\{\delta_1(s)I_n\left(\frac{r\lambda_s}{a}\right)\sin\frac{\lambda_s r}{a}+\sum_{j=1}^{\infty}\left[\delta_2(s,j)\sinh\frac{\alpha_{nj} r}{a}+\delta_3(s,j)\cosh\frac{\alpha_{nj} r}{a}\right]J_n\left(\frac{\alpha_{nj} r}{a}\right)\right\}\dot{W}_s(t) \tag{26}$$

where

$$\delta_1(s)=\frac{-a}{\lambda_s I_n'(\lambda_s)}$$

$$\delta_2(s,j)=\frac{2a\lambda_s}{\alpha_{nj}\left(1-\frac{n^2}{\alpha_{nj}^2}\right)J_n(\alpha_{nj})(\alpha_{nj}^2+\lambda_s^2)}$$

$$\delta_3(s,j)=\frac{2a\left(\alpha_{nj}\sin\frac{\lambda_s b}{a}-\lambda_s\sinh\frac{\alpha_{nj}b}{a}\right)}{\alpha_{nj}\left(1-\frac{n^2}{\alpha_{nj}^2}\right)J_n(\alpha_{nj})(\alpha_{nj}^2+\lambda_s^2)\cosh\frac{\alpha_{nj}b}{a}}$$

DERIVATION OF FREQUENCY EQUATIONS

Upon substitution of u, v, and w as given by equations (17) into equation (8), the following expression for potential energy is obtained:

$$V=\frac{\pi EhL}{4a\,(1-\mu^2)}\sum_{s=0}^{N}\left\{\lambda_s{}^2U_s(t)^2+[nV_s(t)-W_s(t)]^2-2\mu\lambda_sU_s(t)[nV_s(t)-W_s(t)]\right.$$
$$+\frac{1-\mu}{2}[\lambda_sV_s(t)-nU_s(t)]^2+\beta(\lambda_s{}^2+n^2)^2W_s(t)^2+\frac{1-\mu}{2}\frac{pa}{Gh}\left(\frac{\lambda_s{}^2}{2}+n^2\right)W_s(t)^2$$
$$\left.+\frac{1-\mu}{2}\frac{\rho_l}{2}\frac{a}{Gh}n^2\left(\frac{b}{L}\right)^2\left[K_2(s)W_s(t)^2+\sum_{\substack{k=0\\k\neq s}}^{N}K_1(s,k)W_k(t)W_s(t)\right]\right\} \tag{27}$$

where

$$K_1(s,k)=\left[1-2\frac{1-\cos(\lambda_s+\lambda_k)\frac{b}{a}}{\frac{b^2}{a^2}(\lambda_s+\lambda_k)^2}\right]-\left[1-2\frac{1-\cos(\lambda_s-\lambda_k)\frac{b}{a}}{\frac{b^2}{a^2}(\lambda_s-\lambda_k)^2}\right] \tag{28}$$

$$K_2(s)=1-2\frac{1-\cos\frac{2\lambda_sb}{a}}{\left(\frac{2\lambda_sb}{a}\right)^2} \tag{29}$$

$$\lambda_s=\frac{(m+s)\pi a}{L}$$

$$\lambda_k=\frac{(m+k)\pi a}{L}$$

The potential function Φ (eq. (26)) is now substituted into equation (16) to obtain the kinetic energy of the liquid. This result is combined with the kinetic energy of the shell, determined by substitution of the displacements (eq. (17)) into equation (9). The total kinetic energy thus obtained is given by

$$T=\frac{\pi\rho_chaL}{4g}\sum_{s=0}^{N}\left\{\left[1+\frac{\rho_lab}{\rho_chL}m_{v1}(s)\right]\dot{W}_s(t)^2+\frac{\rho_lab}{\rho_chL}\sum_{\substack{k=0\\k\neq s}}^{N}m_{r2}(s,k)\dot{W}_k(t)\dot{W}_s(t)\right\} \tag{30}$$

where

$$m_{v1}(s)=f_n(\lambda_s)\left[1-\frac{\sin\frac{2\lambda_sb}{a}}{\frac{2\lambda_sb}{a}}\right]+\frac{a\lambda_sf_n(\lambda_s)^2\sin\frac{2\lambda_sb}{a}}{2b}\left[1-\frac{I_{n-1}(\lambda_s)I_{n+1}(\lambda_s)}{I_n(\lambda_s)^2}\right]$$
$$-\sum_{j=1}^{\infty}\frac{4a\left\{2\lambda_s\alpha_{nj}\sin\frac{\lambda_sb}{a}+\left[\alpha_{nj}{}^2\sin^2\left(\frac{\lambda_sb}{a}\right)-\lambda_s{}^2\right]\sinh\frac{\alpha_{nj}b}{a}\right\}}{b\alpha_{nj}\left(1-\frac{n^2}{\alpha_{nj}{}^2}\right)(\alpha_{nj}{}^2+\lambda_s{}^2)\cosh\frac{\alpha_{nj}b}{a}} \tag{31}$$

$$m_{r2}(s,k)=f_n(\lambda_s)\left[\frac{\sin(\lambda_s-\lambda_k)\frac{b}{a}}{(\lambda_s-\lambda_k)\frac{b}{a}}-\frac{\sin(\lambda_s+\lambda_k)\frac{b}{a}}{(\lambda_s+\lambda_k)\frac{b}{a}}\right]$$

$$+\frac{a\lambda_k\lambda_s^2\sin\frac{\lambda_k b}{a}\cos\frac{\lambda_s b}{a}f_n(\lambda_s)f_n(\lambda_k)[I_{n-1}(\lambda_s)I_{n+1}(\lambda_k)-I_{n-1}(\lambda_k)I_{n+1}(\lambda_s)]}{nb(\lambda_k^2-\lambda_s^2)I_n(\lambda_s)I_n(\lambda_k)}$$

$$-\sum_{j=1}^{\infty}\left\{\frac{4a\left(\lambda_s\sin\frac{\lambda_k b}{a}\cos\frac{\lambda_s b}{a}-\lambda_k\sin\frac{\lambda_s b}{a}\cos\frac{\lambda_k b}{a}\right)}{b\left(1-\frac{n^2}{\alpha_{nj}^2}\right)(\alpha_{nj}^2+\lambda_s^2)(\alpha_{nj}^2+\lambda_k^2)}\right.$$

$$\left.+\frac{4a\left[\alpha_{nj}\left(\lambda_s\sin\frac{\lambda_k b}{a}+\lambda_k\sin\frac{\lambda_s b}{a}\right)+\left(\alpha_{nj}^2\sin\frac{\lambda_s b}{a}\sin\frac{\lambda_k b}{a}-\lambda_s\lambda_k\right)\sinh\frac{\alpha_{nj}b}{a}\right]}{b\alpha_{nj}^2\left(1-\frac{n^2}{\alpha_{nj}^2}\right)(\alpha_{nj}^2+\lambda_s^2)(\alpha_{nj}^2+\lambda_k^2)\cosh\frac{\alpha_{nj}b}{a}}\right\} \quad (32)$$

and

$$f_n(\lambda_s)=\frac{I_n(\lambda_s)}{\lambda_s I_n'(\lambda_s)}$$

An approximate analysis of the liquid kinetic energy is given in the appendix and leads to the following expressions for $m_{r1}(s)$ and $m_{r2}(s,k)$:

$$m_{r1}(s)=f_n(\lambda_s)\left(1-\frac{\sin\frac{2\lambda_s b}{a}}{\frac{2\lambda_s b}{a}}\right) \quad (33)$$

$$m_{r2}(s,k)=f_n(\lambda_s)\left[\frac{\sin(\lambda_s-\lambda_k)\frac{b}{a}}{(\lambda_s-\lambda_k)\frac{b}{a}}-\frac{\sin(\lambda_s+\lambda_k)\frac{b}{a}}{(\lambda_s+\lambda_k)\frac{b}{a}}\right] \quad (34)$$

For convenience the quantities $m_{r1}(s)$ and $m_{r2}(s,k)$ are termed virtual mass coefficients; the expressions given by equations (31) and (32) are referred to as "exact" virtual mass coefficients; whereas the expressions given by equations (33) and (34) are referred to as approximate virtual mass coefficients. Frequencies have been calculated both by using equations (31) and (32) and by using equations (33) and (34), and comparisons are shown in subsequent sections of this report.

Equations of motion.—Inasmuch as $U_s(t)$, $V_s(t)$, and $W_s(t)$ are independent variables, they may be taken as generalized coordinates and the Lagrange equation applied. A general form of the equations of motion can be obtained if derivatives are taken of the general term of the summations indicated in equations (27) and (30). The equations of motion are obtained by the application of Lagrange's equations:

$$\left.\begin{aligned}\frac{d}{dt}\left[\frac{\partial T}{\partial\dot{U}_s(t)}\right]+\frac{\partial V}{\partial U_s(t)}=0\\ \frac{d}{dt}\left[\frac{\partial T}{\partial\dot{V}_s(t)}\right]+\frac{\partial V}{\partial V_s(t)}=0\\ \frac{d}{dt}\left[\frac{\partial T}{\partial\dot{W}_s(t)}\right]+\frac{\partial V}{\partial W_s(t)}=0\end{aligned}\right\} \quad (35)$$

The resulting equations of motion become, with the assumption of simple harmonic motion $\ddot{W}_s(t)=-\omega^2W_s(t)$:

$$\left(\lambda_s^2+\frac{1-\mu}{2}n^2\right)U_s(t)-n\frac{1+\mu}{2}\lambda_s V_s(t)+\mu\lambda_s W_s(t)=0 \quad (36)$$

$$-n\frac{1+\mu}{2}\lambda_s U_s(t)+\left(n^2+\frac{1-\mu}{2}\lambda_s^2\right)V_s(t)-nW_s(t)=0 \quad (37)$$

and

$$\mu\lambda_s U_s(t)-nV_s(t)+\left\{1+\beta(\lambda_s^2+n^2)^2+\frac{1-\mu}{2}\frac{pa}{Gh}\left(\frac{\lambda_s^2}{2}+n^2\right)+\frac{1-\mu}{2}\frac{\rho_t L}{2}\frac{a}{Gh}\left(\frac{b}{L}\right)^2 n^2 K_2(s)-\Delta\left[1+\frac{\rho_t ab}{\rho_c hL}\,m_{t1}(s)\right]\right\}W_s(t)+\frac{1-\mu}{2}\frac{\rho_t L}{2}\frac{a}{Gh}\,n^2\left(\frac{b}{L}\right)^2\sum_{\substack{k=0\\k\neq s}}^{N}K_1(s,k)\,W_k(t)-\Delta\,\frac{\rho_t ab}{\rho_c hL}\sum_{\substack{k=0\\k\neq s}}^{N}\frac{1}{2}\left[m_{t2}(s,k)+m_{t2}(k,s)\right]W_k(t)=0 \tag{38}$$

where

$$\Delta=\frac{(1-\mu^2)\rho_c a^2\omega^2}{Eg} \tag{39}$$

It can be seen from the strain and kinetic energy expressions (eqs. (27) and (30)) that there will be $(N+1)$ terms in the summations, leading to $3(N+1)$ equations of motion, of which $(N+1)$ equations are of the form of equation (36), another $(N+1)$ equation of the form of equation (37), and the remaining $(N+1)$ equations are of the form of equation (38). The matrix equation representing these $3(N+1)$ equations is

$$\begin{bmatrix}
\lambda_0^2+\frac{1-\mu}{2}n^2 & -n\frac{1+\mu}{2}\lambda_0 & \mu\lambda_0 & 0 & 0 & 0 & \cdots & 0 & 0 & 0\\
n\frac{1+\mu}{2}\lambda_0 & n^2+\frac{1-\mu}{2}\lambda_0^2 & -n & 0 & 0 & 0 & \cdots & 0 & 0 & 0\\
\mu\lambda_0 & -n & q(0) & 0 & 0 & q_1(0,1) & \cdots & 0 & 0 & q_1(0,N)\\
0 & 0 & 0 & \lambda_1^2+\frac{1-\mu}{2}n^2 & -n\frac{1+\mu}{2}\lambda_1 & \mu\lambda_1 & \cdots & 0 & 0 & 0\\
0 & 0 & 0 & -n\frac{1+\mu}{2}\lambda_1 & n^2+\frac{1-\mu}{2}\lambda_1^2 & -n & \cdots & 0 & 0 & 0\\
0 & 0 & q_1(1,0) & \mu\lambda_1 & -n & q(1) & \cdots & 0 & 0 & q_1(1,N)\\
\cdot & \cdot & \cdot & \cdot & \cdot & \cdot & \cdots & \cdot & \cdot & \cdot\\
\cdot & \cdot & \cdot & \cdot & \cdot & \cdot & \cdots & \cdot & \cdot & \cdot\\
\cdot & \cdot & \cdot & \cdot & \cdot & \cdot & \cdots & \cdot & \cdot & \cdot\\
0 & 0 & 0 & 0 & 0 & 0 & \cdots & \lambda_N^2+\frac{1-\mu}{2}n^2 & -n\frac{1+\mu}{2}\lambda_N & \mu\lambda_N\\
0 & 0 & 0 & 0 & 0 & 0 & \cdots & -n\frac{1+\mu}{2}\lambda_N & n^2+\frac{1-\mu}{2}\lambda_N^2 & -n\\
0 & 0 & q_1(N,0) & 0 & 0 & q_1(N,1) & \cdots & \mu\lambda_N & -n & q(N)
\end{bmatrix}\begin{Bmatrix}U_0\\V_0\\W_0\\U_1\\V_1\\W_1\\\cdot\\\cdot\\\cdot\\U_N\\V_N\\W_N\end{Bmatrix}=0 \tag{40}$$

where

$$q(s)=1+\beta(\lambda_s^2+n^2)^2+\frac{1-\mu}{2}\frac{pa}{Gh}\left(\frac{\lambda_s^2}{2}+n^2\right)+\frac{1-\mu}{2}\frac{\rho_t L}{2}\frac{a}{Gh}\left(\frac{b}{L}\right)^2 n^2 K_2(s)-\Delta\left[1+\frac{\rho_t ab}{\rho_c hL}\,m_{t1}(s)\right] \tag{41}$$

$$q_1(s,k)=\frac{1-\mu}{2}\frac{\rho_t L}{2}\frac{a}{Gh}\,n^2\left(\frac{b}{L}\right)^2 K_1(s,k)+\Delta\,\frac{\rho_t ab}{\rho_c hL}\,\frac{1}{2}\left[m_{t2}(s,k)+m_{t2}(k,s)\right] \tag{42}$$

The frequency determinant yielding N natural frequencies is formed from the elements of the characteristic matrix of equation (40). The frequency of principal interest is the lowest frequency, and the higher frequencies introduced by inclusion of several terms in the displacement functions are neglected. Several examples are now considered.

Frequency equation for $N=0$.—If N is set equal to zero, only the first term of the series in equation

(17) is retained and the displacement relations reduce to

$$\left.\begin{aligned} u &= U_0(t)\cos n\varphi \cos\frac{m\pi x}{L} \\ v &= V_0(t)\sin n\varphi \sin\frac{m\pi x}{L} \\ w &= W_0(t)\cos n\varphi \sin\frac{m\pi x}{L} \end{aligned}\right\} \tag{43}$$

The frequency determinant, formed from the first three elements of the first three rows of equation (40), is

$$\begin{vmatrix} \lambda_0^2+\frac{1-\mu}{2}n^2 & -n\frac{1+\mu}{2}\lambda_0 & \mu\lambda_0 \\ -n\frac{1+\mu}{2}\lambda_0 & n^2+\frac{1-\mu}{2}\lambda_0^2 & -n \\ \mu\lambda_0 & -n & q(0) \end{vmatrix}=0 \tag{44}$$

where

$$q(0)=1+\beta(\lambda_0^2+n^2)^2+\frac{1-\mu}{2}\frac{pa}{Gh}\left(\frac{\lambda_0^2}{2}+n^2\right)+\frac{1-\mu}{2}\frac{\rho_l La}{2Gh}\left(\frac{b}{L}\right)^2 n^2K_2(0)-\Delta\left[1+\frac{\rho_l ab}{\rho_c hL}m_{r1}(0)\right] \tag{45}$$

Equation (44) can be expanded and combined with equation (45) to give the following relatively simple expression for the frequency factor Δ; thus,

$$\Delta=\frac{(1-\mu^2)\lambda_0^4+\beta(n^2+\lambda_0^2)^2+\frac{(1-\mu)pa}{2Gh}\left(n^2+\frac{\lambda_0^2}{2}\right)+\frac{(1-\mu)\rho_l aL}{4Gh}\left(\frac{b}{L}\right)^2 n^2K_2(0)}{(n^2+\lambda_0^2)^2\left[1+\frac{\rho_l ab}{\rho_c hL}m_{r1}(0)\right]} \tag{46}$$

where

$$K_2(0)=1-2\left[\frac{1-\cos\frac{2m\pi b}{L}}{\left(\frac{2m\pi b}{L}\right)^2}\right] \tag{47}$$

The first three terms of the numerator of equation (46) represent the contribution to the frequency of middle surface elasticity, wall bending, and internal pressure, respectively. The fourth term of the numerator and the second term of the denominator represent, respectively, the contributions to frequency of hydrostatic pressure of the liquid and the effective mass of the liquid. When the liquid depth b is zero, equation (46) reduces to

$$\Delta=\frac{(1-\mu^2)\lambda^4}{(n^2+\lambda^2)^2}+\beta(n^2+\lambda^2)^2+\frac{(1-\mu)pa}{2Gh}\left(n^2+\frac{\lambda^2}{2}\right) \tag{48}$$

Equation (48) has been derived and discussed previously (refs. 4 and 9) using different derivation procedures.

When values of $m_{v1}(0)$ and $K_2(0)$ from equations (31) and (47) are substituted into equation (46) and the liquid depth b is equal to the length L, equation (46) becomes

$$\Delta=\frac{\dfrac{(1-\mu^2)\lambda_0^4}{(n^2+\lambda_0^2)^2}+\beta(n^2+\lambda_0^2)^2+\dfrac{(1-\mu)\rho a}{2Gh}\left(n^2+\dfrac{\lambda_0^2}{2}\right)+\dfrac{(1-\mu)\rho_l aLn^2}{4Gh}}{1+\dfrac{\rho_l a f_n(\lambda_0)}{\rho_c h}+\dfrac{4\rho_l a^2\lambda_0^2}{\rho_c hL}\displaystyle\sum_{j=1}^{\infty}\frac{\tanh\dfrac{\alpha_{nj}L}{a}}{\alpha_{nj}\left(1-\dfrac{n^2}{\alpha_{nj}^2}\right)(\alpha_{nj}^2+\lambda_0^2)^2}} \tag{49}$$

Equation (49) is quite similar to a frequency equation derived in reference 5. The equation of reference 5, when the fluid is considered to be incompressible, reduces to equation (49) with the fourth term of the numerator and the third term of the denominator deleted. These terms represent, respectively, the effect of the hydrostatic pressure of the liquid, and an effect of finite cylinder length. Neither effect was considered in reference 5.

Frequency equation for $N=1$.—If $N=1$, two terms of the series in the displacement expressions are retained and the displacements are given by

$$\left.\begin{aligned} u&=\left[U_0(t)\cos\frac{m\pi x}{L}+U_1(t)\cos\frac{(m+1)\pi x}{L}\right]\cos n\varphi\\ v&=\left[V_0(t)\sin\frac{m\pi x}{L}+V_1(t)\sin\frac{(m+1)\pi x}{L}\right]\sin n\varphi\\ w&=\left[W_0(t)\sin\frac{m\pi x}{L}+W_1(t)\sin\frac{(m+1)\pi x}{L}\right]\cos n\varphi \end{aligned}\right\} \tag{50}$$

The frequency determinant is now formed from the first six rows of the first six columns of the square matrix of equation (40) and is given by

$$\begin{vmatrix} \lambda_0^2+\frac{1-\mu}{2}n^2 & -n\frac{1+\mu}{2}\lambda_0 & \mu\lambda_0 & 0 & 0 & 0\\ -n\frac{1+\mu}{2}\lambda_0 & n^2+\frac{1-\mu}{2}\lambda_0^2 & -n & 0 & 0 & 0\\ \mu\lambda_0 & -n & q(0) & 0 & 0 & q_1(0,1)\\ 0 & 0 & 0 & \lambda_1^2+\frac{1-\mu}{2}n^2 & -n\frac{1+\mu}{2}\lambda_1 & \mu\lambda_1\\ 0 & 0 & 0 & -n\frac{1+\mu}{2}\lambda_1 & n^2+\frac{1-\mu}{2}\lambda_1^2 & -n\\ 0 & 0 & q_1(1,0) & \mu\lambda_1 & -n & q(1) \end{vmatrix}=0 \tag{51}$$

In this equation $q(0)$ is given by equation (45) and

$$q(1)=1+\beta(\lambda_1^2+n^2)^2+\frac{1-\mu}{2}\frac{\rho a}{Gh}\left(\frac{\lambda_1^2}{2}+n^2\right)+\frac{1-\mu}{2}\frac{\rho_l L}{2}\frac{a}{Gh}\left(\frac{b}{L}\right)^2 n^2K_2(1)-\Delta\left[1+\frac{\rho_l ab}{\rho_c hL}m_{v1}(1)\right] \tag{52}$$

$$q_1(1,0)=\frac{1-\mu}{2}\frac{\rho_l L}{2}\frac{a}{Gh}n^2\left(\frac{b}{L}\right)^2K_1(1,0)-\Delta\frac{\rho_l ab}{\rho_c hL}\frac{1}{2}\left[m_{v2}(1,0)+m_{v2}(0,1)\right] \tag{53}$$

$$K_1(1,0)=\left\{1-2\frac{1-\cos(2m+1)\frac{\pi b}{L}}{\left[(2m+1)\frac{\pi b}{L}\right]^2}\right\}-\left[1-2\frac{1-\cos\frac{\pi b}{L}}{\left(\frac{\pi b}{L}\right)^2}\right] \quad (54)$$

$$K_2(1)=1-2\frac{1-\cos(m+1)\frac{2\pi b}{L}}{\left[(m+1)\frac{2\pi b}{L}\right]^2} \quad (55)$$

With the use of equations (45) and (52) to (55), equation (51) can be solved for the frequency parameter Δ by using known methods; the required quantities are the shell dimensions (a, h, and L), shell material (E, μ, and ρ_c), liquid density and depth (ρ_l and b), and the mode shape (defined by m and n). The value of Δ from the solution of equation (46) or (51) can be substituted into equation (39) to give the frequency of the vibration. As illustrated in these examples, any number of terms of the series in the displacement expressions (eq. (17)) may be taken and the resulting $3(N+1)$ by $3(N+1)$ determinant may be solved for the frequency.

EXPERIMENTS

GENERAL REMARKS

Natural frequencies and node lines of two thin-walled cylinders were determined experimentally for comparison with the calculated results. A few mode shapes and some values of damping were also determined. The ratios of the cylinder radius to the wall thickness were 937 and 3,000; the ends were attached to relatively rigid structures and were therefore considered to be fixed. The natural frequencies and node lines were determined with internal pressures up to 8 psig and for ratios of water depth to cylinder length b/L from 0 to 1.47. The mode shapes were determined for values of b/L of 0.25 and 0.50, and the damping was determined with the cylinder empty and filled with water.

APPARATUS

Cylinders.—The physical characteristics of the two thin-walled, unstiffened, circular cylinders used in these tests are given in the following table:

Parameter	Cylinder 1	Cylinder 2
Material	Aluminum (2014–T6)	Steel (stainless)
Weight density, ρ, lb/cu in.	0.10	0.28
Young's modulus, E, lb/sq in.	10×10^6	30×10^6
Poisson's ratio, μ	0.33	0.30
Length, L, in.	28.6	22.0
Mean radius, a, in.	15.0	12.0
Skin thickness, h, in.	0.016	0.004
Radius-thickness ratio, a/h	937	3,000
Radius-length ratio, a/L	0.525	0.546

Photographs of the cylinders in the testing position are shown in figure 3. The ends of the cylinders were riveted to 1-inch by 1-inch by ⅛-inch aluminum angle rings, which held the cylinder ends at essentially a zero deflection and zero slope condition. The cylinders were closed at the top by fiberglass domes and at the bottom by aluminum cones (not visible in figure). Fittings for pressurization and for water filling and draining were located on the domes and on the cones.

Shaker.—An alternating force for excitation of the cylinders was provided by an air shaker such as described in reference 12. The shaker output is basically a jet of air which is interrupted by teeth on a rotating disk. The magnitude of the alternating force is controlled by the pressure of the air fed to the jet, and the frequency of the force is controlled by the speed of rotation and the number of teeth on the disk. This type of shaker was selected because it provided an alternating force without adding a large concentrated mass to the model.

TEST PROCEDURE

Frequencies and node lines.—The test setup is shown in figure 3. The shaker was placed in the position expected to give maximum response of the cylinder in the desired mode. For instance, when the cylinder was empty and it was desired to excite the first axial mode ($m=1$), the shaker was placed midway between the ends of the cylinder; when the second axial mode ($m=2$) was desired the shaker was placed at a distance of about one-fourth of the length from one end.

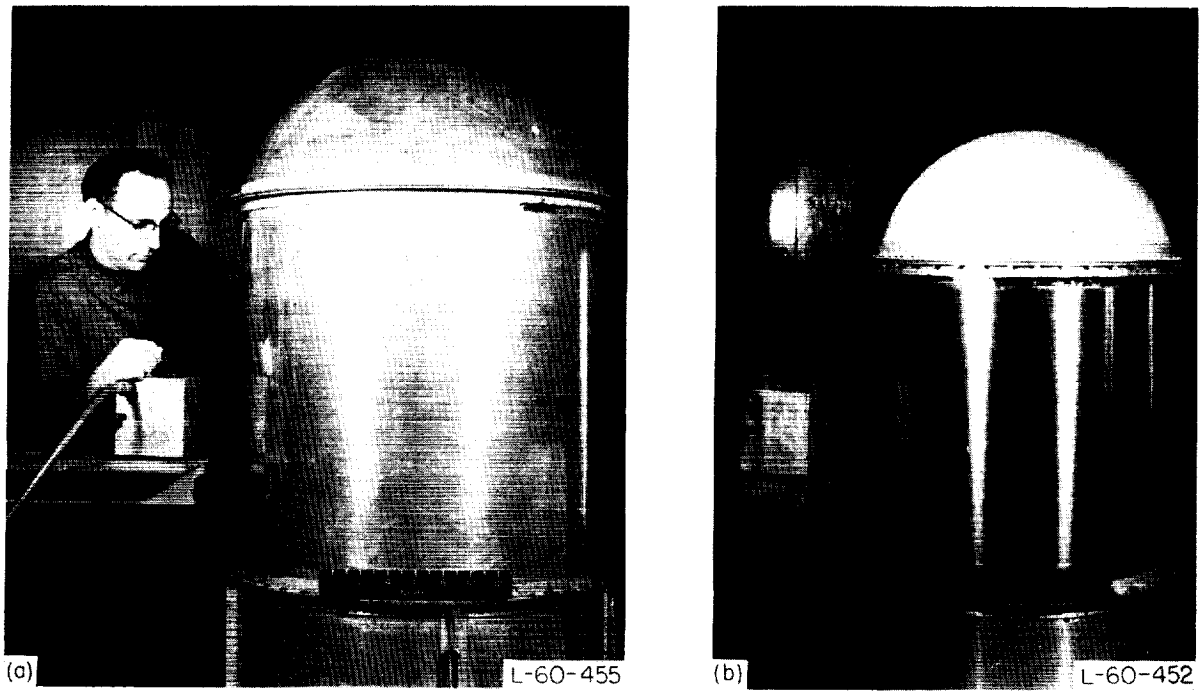

(a) Cylinder 1. (b) Cylinder 2.

FIGURE 3.—View of test cylinders and test setup.

The circumferential position of the shaker did not appear to have any effect on the response.

With the shaker in position and the output force constant, the applied excitation frequency was varied until a maximum response was obtained. Maximum response was identified by touching the cylinder lightly with the fingertips while varying the frequency of the applied force. The mode was then identified by locating the node lines, which, in this case, are positions of little or no radial motion. (The tangential motions are not necessarily zero at these nodes.) The node lines were also identified by touch. When the fingertips were moved along the length or around the circumference of the cylinder, the positions of smallest amplitude, in most cases, could be easily felt, and the number of node lines determined. Touching the cylinder lightly did not appear to change appreciably the amplitude of the response of cylinder 1 under any condition, nor of cylinder 2 when it was pressurized or contained liquid. When cylinder 2 was empty and unpressurized, however, it was not possible to identify the natural modes or frequencies because of the initial imperfections and local flexibility of this very thin cylinder.

Mode shapes.—A miniature accelerometer (weight, 0.14 oz) was used to determine axial mode shapes. With the cylinder vibrating in a resonant condition the accelerometer was attached to the cylinder wall with double-backed tape, and the output was read from a voltmeter. This reading was taken with the accelerometer attached at several points along the cylinder length, and all the readings for that mode were divided by the largest reading to give a normalized mode shape. The accelerometer output was fed to an amplifier, then to a band-pass filter to remove unwanted harmonics, and finally to a root-mean-square voltmeter, which indicated the amplitude of the vibration.

Damping.—Damping data were obtained only on cylinder 1 ($a/h=937$); the procedure for obtaining the data was as follows. The cylinder was forced to vibrate in a resonant condition and then the shaker was shut off as suddenly as possible by closing the air supply valve. The damping measurements were obtained from the output of the miniature accelerometer attached to the cylinder wall, the output being recorded on an oscillograph. A smooth curve was faired through the peaks of the decaying response and the

damping factor was determined from the relation:

$$g_1=\frac{1}{\pi\nu}\log_e\frac{w_t}{w_{\left(t+\frac{\nu}{f}\right)}} \tag{56}$$

where

w_t amplitude at time t

$w_{\left(t+\frac{\nu}{f}\right)}$ amplitude ν cycles later

f natural frequency of vibration

RESULTS

Frequencies.—The experimentally determined natural frequencies are presented in tables I and II and are discussed in conjunction with the theory in the subsequent section "Comparison of Theoretical and Experimental Frequencies."

Mode shapes.—The experimentally determined mode data are presented in tables III and IV and in figures 4 and 5. Experimental axial mode shapes of cylinder 2 for an internal pressure of 8 psig are shown in figure 4 for $m=1$, $b/L=0.25$, and for $m=2$, $b/L=0.50$ at several values of n. This figure shows the mode shapes to be nonsymmetrical, with the largest amplitudes occurring below the water line. The results show further that the mode shapes vary considerably with the value of n. For the smaller values of n the amplitude is approximately the same both below and above the water line, but as n increases, the relative amplitude above the water line decreases until at the largest values of n shown, the amplitude above the water line is negligible.

Also of interest with respect to the modes is the position of the circumferential node line. In figure 4(b), ($m=2$) the circumferential node line (defined by the position of zero relative amplitude) is shown to be at about one-half the liquid depth for all values of n. The variation with internal pressure of the ratio of the circumferential node-line heights above the tank bottom x_1 and x_2 to the water depth b is shown in figure 5. This figure shows that, in general, the node lines are about evenly distributed over the water depth; when $m=2$ the node-line height x_1 is about half of the water depth, and when $m=3$ the node-line heights x_1 and x_2 are about one-third and two-thirds of the water depth, respectively. The effect of an increase of the internal pressure is to decrease slightly both the scatter and the value of the ratio of node-line height to water depth.

Damping.—It was expected that liquid-filled cylinders would have more relative damping than empty cylinders so that the resonant peaks would be more difficult to distinguish and the decay of the vibration would be more rapid when the exciting force was removed; however, the experimental results did not show this to be the case. On the contrary, the modes and frequencies of the liquid-filled cylinders were just as easy to excite and identify as those of the empty cylinder. A limited number of damping measurements were made on cylinder 1 at pressures of 1, 4, and 8 psig with the cylinder both empty and water filled. (The mode shapes at which the damping was determined were not identified.) The resulting averages of the damping factors obtained were 0.005 and 0.002 for the empty and water-filled cylinder, respectively. Thus, these values indicate that the damping decreased with the addition of the water.

Tangential and symmetric modes.—During the experiments it was found that the only modes which could be excited were the radial shell modes. The high-frequency axial and tangential modes discussed in reference 7 were never observed. An attempt was made to excite longitudinal vibrations such as those which might be experienced by a liquid-fueled rocket under the transient longitudinal loads at lift-off. In this mode the shell is thought to expand and contract symmetrically while the fluid center of gravity moves vertically. Several shaker orientations were used, but this mode could not be excited with the cylinders and test equipment available.

With the cylinder full of water a mode which appeared to be symmetrical was excited; that is, the amplitude appeared to be the same at all points around the circumference. This amplitude was observed visually on a thread glued around a circumference of the cylinder. However, when the thread was illuminated by the light from a Strobotac, the vibration was found to consist of a series of waves traveling at high speed around the cylinder circumference. It was then determined that this "traveling wave" phenomenon occurred in the region of maximum response of a given mode; at frequencies on either side of this region the waves were stationary.

661671—63——3

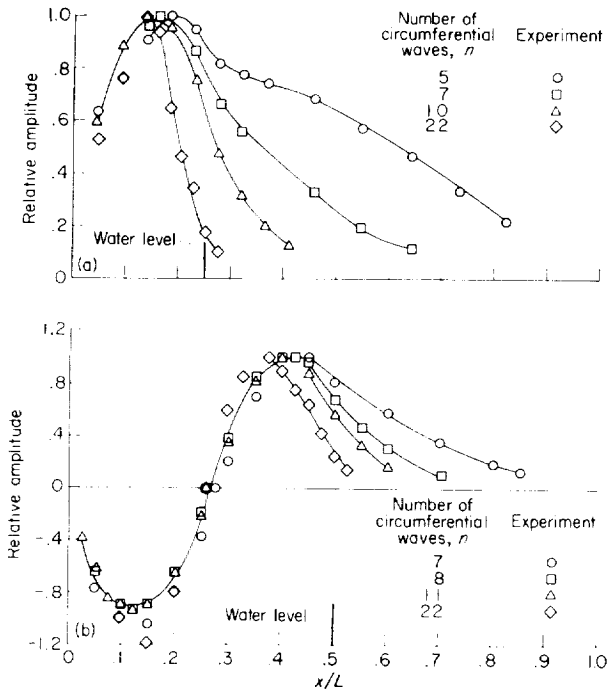

(a) First axial mode. $m=1$; $b/L=0.25$.

(b) Second axial mode. $m=2$; $b/L=0.50$.

FIGURE 4.—Normalized axial vibration mode shapes. Cylinder 2; $a/h=3{,}000$; $p=8$ psig.

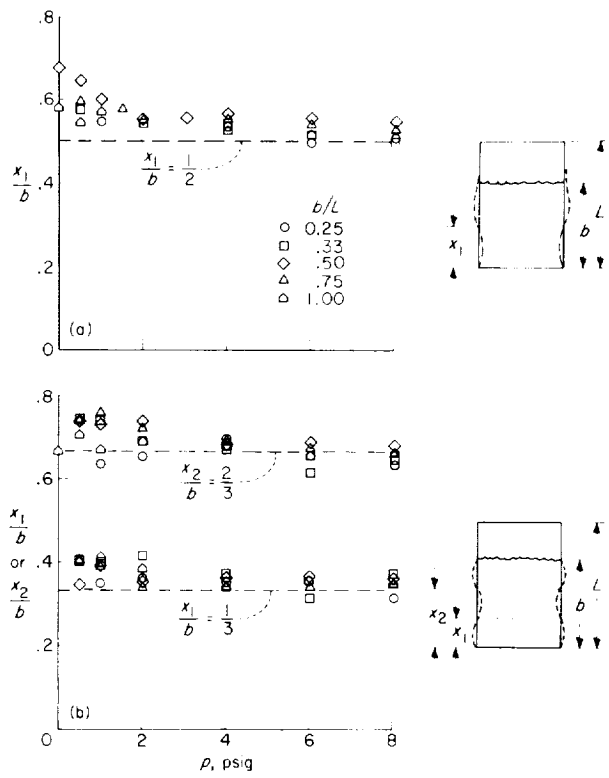

(a) $m=2$.

(b) $m=3$.

FIGURE 5.—Experimental location of circumferential node lines with respect to water depth as function of internal pressure for random values of n. Cylinder 2; $a/h=3{,}000$.

Multiple response.—An interesting phenomenon was observed during tests of the steel cylinder 2 ($a/h=3{,}000$) partly filled with water. In a few cases, two distinct tones could be heard when the cylinder was driven at a particular frequency. When the observer listened to the response with the ear very close to the cylinder, one tone was determined to come from the part of the cylinder above the water line and the other tone from the part below the water line. Further investigation showed that each of the two sections of the cylinder, above and below the water line, could be made to respond relatively independent of the other; that is, the maximum amplitude could be made to occur either above or below the water line. Figure 6 shows the minimum resonant frequency of each section of the cylinder plotted as a function of water depth for several values of internal pressure. For the minimum frequency the measured value of m was always 1, but the value of n varied with the water depth. (These data are also presented in table V.) The figure shows that as water depth increases, the frequency of the section below the water line decreases, but the frequency of the section above the water line increases sharply, as could be expected from the decreasing length of the unfilled part of the cylinder. It can be seen that for some combination of internal pressure and water depth there can be a mode of the lower section which has a frequency that is an even multiple of the frequency of a mode of the upper section. In this case both modes may be excited by the same driving frequency, as was observed in the tests.

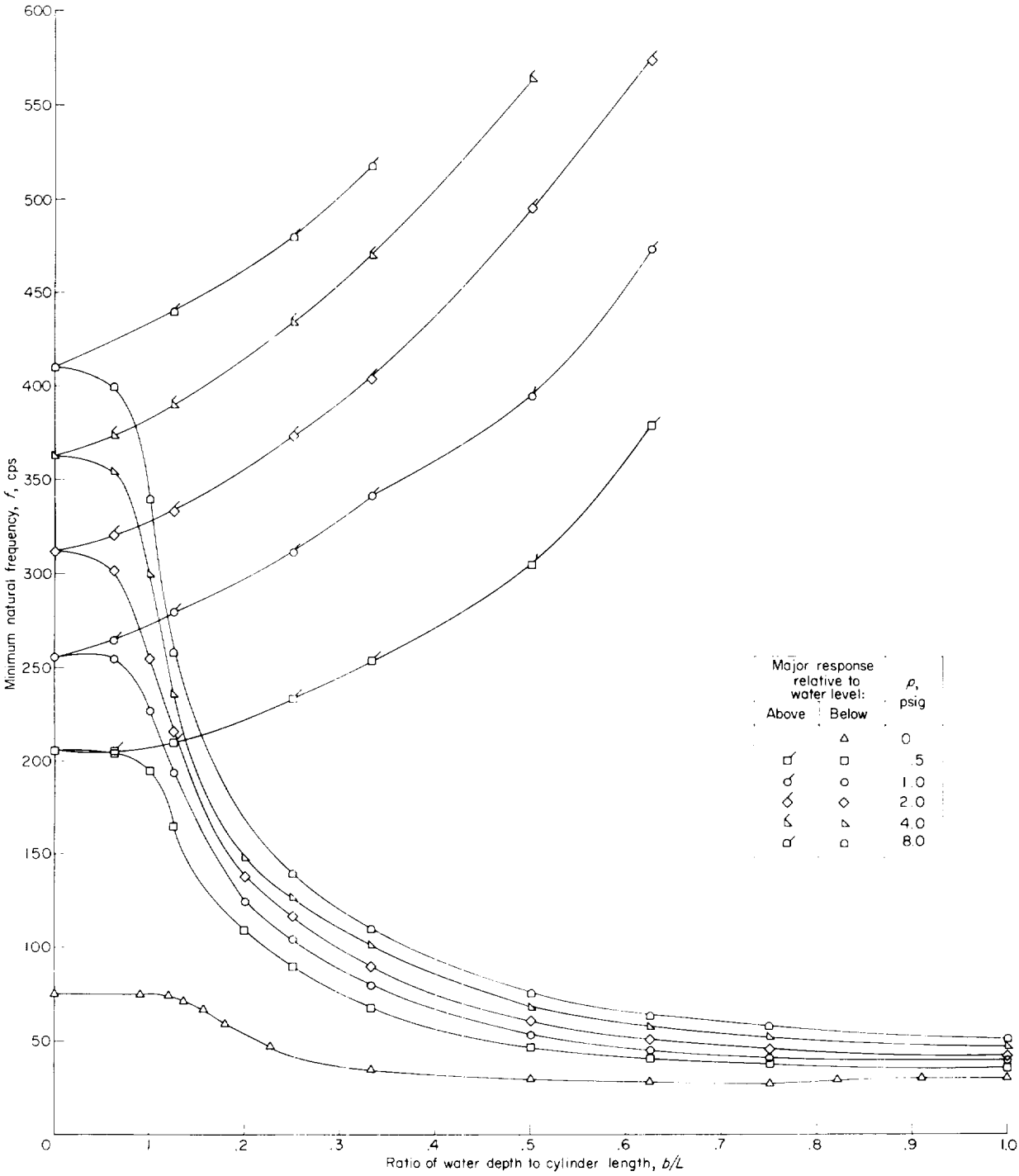

FIGURE 6. Experimental variation of minimum natural frequency with water depth-length ratio showing multiple response. Cylinder 2; $a/h = 3{,}000$; $m = 1$.

TABLE I

EXPERIMENTAL NATURAL FREQUENCIES OF CYLINDER 1

m	p, psig	f, cps, at $n=$: 3	4	5	6	7	8	9	10	11	12	13	14	15	16	17	18	19	20	21
$b/L=0$																				
1	0	----	----	----	----	----	154	129	117	115	122	132	143	163	184	209	237	255	----	---
	1	----	----	----	----	205	201	214	223	244	----	286	308	335	----	----	----	----	----	---
	2	----	----	----	236	244	252	273	292	320	345	373	410	----	----	----	----	----	----	---
	4	----	----	291	284	303	325	362	394	441	----	----	----	----	----	----	----	----	----	---
	8	----	319	326	352	385	440	494	---	594	----	----	----	----	----	----	----	----	----	---
2	0	----	----	----	----	----	----	----	246	---	----	200	202	207	219	235	253	---	300	---
	1	----	----	----	----	----	----	----	----	309	----	326	342	----	----	405	----	----	----	---
3	0	----	----	----	----	----	----	----	----	----	----	----	----	280	----	----	----	----	----	328
$b/L=0.15$																				
1	0	----	----	----	----	---	----	----	90.0	----	----	----	----	112	----	----	----	----	----	---
$b/L=0.25$																				
1	0	----	----	----	----	----	----	----	56.0	----	58.2	----	63.8	68.0	71.5	75.3	80.0	84.0	88.1	---
$b/L=0.38$																				
1	0	----	----	----	----	----	----	----	37.1	39.1	41.4	44.5	48.2	52.3	58.7	64.2	69.8	75.5	----	---
$b/L=0.50$																				
1	0	----	----	----	---	27.0	27.3	28.3	30.1	32.2	35.2	39.5	43.8	48.9	54.3	61.1	68.0	74.1	81.5	---

TABLE I

EXPERIMENTAL NATURAL FREQUENCIES OF CYLINDER 1—Concluded

m	p, psig	f, cps, at $n=$: 3	4	5	6	7	8	9	10	11	12	13	14	15	16	17	18	19	20	21
									$b/L=0.75$											
1	0	----	----	----	----	----	23. 5	24. 5	27. 0	30. 0	33. 2	38. 0	42. 2	47. 6	53. 4	59. 7	66. 6	74. 9	82. 5	---
									$b/L=1.00$											
1	0	----	----	----	----	24. 0	25. 0	27. 0	30. 0	34. 0	37. 6	41. 5	47. 5	52. 2	58. 7	64. 2	69. 8	----	----	---
	4	---	37. 0	38. 0	42. 0	47. 1	56. 0	65. 0	75. 6	86. 3	97. 8	----	123	135	---	---	----	----	----	---
	8	41. 6	40. 5	45. 0	52. 7	63. 6	75. 2	88. 6	103	117	132	148	----	----	----	----	----	----	----	---
3	4	----	----	----	----	----	----	----	----	----	----	130	----	----	----	----	----	----	----	---
	8	----	----	----	----	----	----	----	----	----	----	144	----	----	----	----	----	----	----	---
									$b/L=1.09$											
1	0	----	----	----	27. 5	27. 1	28. 5	30. 0	32. 0	36. 0	39. 7	----	50. 5	57. 0	62. 9	69. 0	76. 5	----	93. 2	---
2	0	----	----	----	----	----	----	----	53. 2	----	55. 0	58. 0	----	67. 8	73. 5	80. 7	88. 0	96. 0	----	---
3	0	----	----	----	----	----	----	----	----	----	----	78. 3	79. 1	82. 0	85. 5	91. 5	97. 7	105	----	---
									$b/L=1.47$											
1	0	----	----	----	29. 5	----	32. 6	35. 1	39. 5	44. 9	49. 8	55. 2	----	69. 0	----	----	----	----	----	---
2	0	----	----	----	----	----	----	----	56. 8	58. 2	----	66. 1	71. 2	79. 0	86. 0	94. 8	101	----	----	---
3	0	----	----	----	----	----	----	----	----	----	87. 2	86. 2	87. 1	91. 9	97. 3	103	111	121	132	---

TABLE II

EXPERIMENTAL NATURAL FREQUENCIES OF CYLINDER 2

m	p, psig	f, cps, at $n=$:																										
		4	5	6	7	8	9	10	11	12	13	14	15	16	17	18	19	20	21	22	23	24	25	26	27	28	29	30
$b/L=0$																												
1	0.5						206	211	219	229	240	250	266	279	300	319	337											
1	1					252	261	272	292	316	341	366	387	416	444	473	500											
1	2				313	325	345	375	407	446	481	515	555	597														
1	4			364	371	393	426	466	514	566	611	675																
1	8	416	430	459	520	575	646	715	787	867																		
2	1										400		427		487	518												
$b/L=0.25$																												
1	0.5										88	91	94	97	100	102	108	112	119	124	130	137	144	151	160	167	175	182
1	1								101	104	108	112	116	122	127	133	138	145	151	159	168	175	184	194	203	213		
1	2				114	115	116	118	122	128	133	140	147	155	164	174	183	192	205	217	230	242						
1	4			127	128	131	135	141	148	158	168	180	192	203	217	232	249	263	279									
1	8		135	139	145	157	166	178	190	204	220	237	255	274	297													
2	2													252	255	260	265	272	276	282	290	299						
2	4									290			296		308	317	326	336	350	364	377	390						
2	8							329	333	342	352	363	375	389	405													

TABLE II

EXPERIMENTAL NATURAL FREQUENCIES OF CYLINDER 2—Continued

m	p, psig	f, cps, at n = : 4	5	6	7	8	9	10	11	12	13	14	15	16	17	18	19	20	21	22	23	24	25	26	27	28	29	30
b/L = 0.50																												
1	0									Minimum frequency = 28.0																		
	.5						47.0	49.5	52.5	55.0	60.0	63.0	68.0	73.5	78.5	85.5												
	1					54.0	56.7	60.5	66.5	70.9	75.9	83.0	90.5	98.3	105	113												
	2			60.0	61.2	65.0	70.5	78.0	85.5	92.0	101	111	120	131	142	154												
	4		68.0	70.5	74.9	82.5	91.2	101	113	124	137	151	166	180	191	213												
	8	76.5	78.7	85.0	95.3	106	120	136	152	170	188		230															
2	0									Minimum frequency = 73.0																		
	.5									Minimum frequency = 102																		
	1										118	120	122	126	130	135	143	150	158	167	175	185	195					
	2								135	136	139	145	151	158	167	176	186	197	208	220	232							
	4							156	159	164	173	184	194	206	220	234	250											
	8				178	180	183	187	198	210	225	241	258	276														
3	2													204	208	213	217	225	238	251	268							
	4											244	251	260	270	295												
	8							280	283	286	291	298	312	328	350													
b/L = 0.75																												
1	0						28.5	29.0																				
	.5				37.0	37.8	39.0	42.3	46.0	50.5	56.0	61.5	67.0	73.0														
	1				42.0	44.3	48.0	53.0	59.0	65.0	72.0	80.7	88.0	96.0	104	112												
	2		45.5	47.0	49.8	55.0	61.5	69.0	78.0	87.5	96.0	107	118	130	142	154												
	4	52.0		56.0	62.5	71.5	80.5	93.0	105	118	133	147	163	179	195	211												
	8	58.0	61.8	70.0	80.8	95.5	111	127	145	164	184	204	226	247														
2	0.5												82.0	88.0	92.5	98.0	106	112	119									
	1							80.0	81.5	84.0	90.0	94.0	100	108	116	124	134											
	2			99.0		93.0		94.0	99.0	105	113	122	130	140	152	162	174											
	4			111		107		117	125	135	147	160	173	189	204	220	236	254	272									
	8			121	123	129	137	150		180	198	216	237	258	280													
3	0														88.0													
	.5									104		107	109	110	114	117	122	126	131	138								
	1											123	126	128	134	140	147	154	162									
	2									142	144	148	154	161	168	180												
	4						162	164	169	177	186	198	208															
	8						188		201	213	226	242																

TABLE II

EXPERIMENTAL NATURAL FREQUENCIES OF CYLINDER 2—Concluded

m	p, psig	f, cps, at n = : 3	4	5	6	7	8	9	10	11	12	13	14	15	16	17	18	19	20	21
$b/L = 1.00$																				
1	0							30.7	32.0	34.5	37.5	40.3	43.8	45.9	49.9					
	.5					35.9	37.3	40.0	43.0	48.5	53.3	58.4								
	1				38.8	40.0	44.0	48.4	53.8	60.0	67.0	74.8	82.0							
	2			42.0	44.0	47.3	53.7	60.0	68.5	78.0	88.0	97.5	108							
	4		46.5	48.3	52.5	60.0	69.5	80.0	92.0	105	118									
	8		51.5	56.5	66.5	79.0	93.0	108	126	144	163									
2	0									55.5	57.0	59.0								
	.5								65.0	68.0	69.0	72.5	77.0	83.0	89.0					
	1							72.0	74.0	76.0	80.2	86.0	91.9	100	108	115				
	2						81.0	82.0	85.0	91.0	98.0	107	117	127	138	151				
	4					91.0	93.0	99.0	106	115	128	140	145	170						
	8				103	105	114	125	140	155	172	191								
3	0.5													95.0	98.5	106	112	119		133
	1										104	105	109		119	126	136			
	2								117	118	122	126	132	141	150	160	170	183		
	4							134	136	141	148	158	168	181	197					
	8							158	166	177	192	208	225							
$b/L = 1.47$																				
1	0					37.0	38.0	45.0			53.0		64.0							
	.5				40.0		44.0		53.0		65.0		80.0							
	1					46.0	49.8	55.7	62.0	68.5	77.0	86.0	95.0	105						
	2			45.0	46.5	51.9	58.5		76.0		95.8		118							
	4		49.0	50.0	55.8		74.0		98.0		124		156							
	8	50.9	54.0	59.0	68.5		97.0	112	130	148	169	189	211							
2	0				84.0	78.0		71.0	70.0	68.0				75.0			85.0			108
	.5								71.8	73.8	77.0	83.0	89.8	96.3	104	112				
	1						77.0	79.0	81.0	84.0	87.0	95.0	103	112	120					
	2						79.0	83.8	90.0	96.3	104	114	125	136	148	161	174			
	4				91.0	92.0	95.0	101	110	121	133	146	161	176	193	209				
	8				103	108	115	127	141	158	175	194	216	237						
3	0											95.0		91.5			97.0			
	.5											106	105.9	110	115	122	129		146	156
	1									111	112	114	118	124	131	140	152	161		
	2								127			132	139	149	159	170				
	4						140			145	152	164	177	189	203					
	8						152	159	168	180	194	210		249						

TABLE III

EXPERIMENTAL AXIAL MODE SHAPES
FOR CYLINDER 2. p 8 psig

(a) b/L 0.25, m 1

x/L	Relative amplitude at n :							
	5	6	7	8	10	11	12	22
0. 045	0. 64			0. 57	0. 60	0. 55	0. 59	0. 53
. 092	. 77			. 81	. 89	. 86	. 83	. 77
. 137	. 91		. 96	. 95	1. 00	1. 00	1. 00	1. 00
. 160			1. 00					. 94
. 183	1. 00	1. 00		1. 00	. 96	. 93	. 88	. 65
. 205							. 60	. 47
. 227	. 95	. 91	. 87	. 81	. 76	. 72	. 48	. 35
. 251								. 18
. 274	. 82	. 76	. 67	. 64	. 48	. 42	. 33	. 11
. 320	. 78	. 69	. 56	. 50	. 32	. 25		
. 365	. 75	. 64		. 43	. 21	. 15		
. 410					. 13			
. 455	. 69	. 49	. 33	. 27				
. 545	. 58	. 35	. 20					
. 640	. 47	. 24	. 12					
. 730	. 35							
. 820	. 23							

(b) b/L 0.50, m 2

x/L	Relative amplitude at n :			
	7	8	11	22
0. 025			−0. 40	
. 05	−0. 78	−0. 65	−. 62	
. 075			−. 85	
. 100	−1. 00	−. 90	−. 90	−1. 00
. 125		−. 94	−. 94	
. 150	−1. 05	. 90		−1. 20
. 200	−. 80	−. 65	−. 65	−. 80
. 250	−. 37	−. 20	−. 22	
. 260		0	0	0
. 275	0			
. 300	. 20	. 37	. 35	. 60
. 325				. 86
. 350	. 70	. 85	. 82	
. 375				1. 00
. 400	1. 00	1. 00	1. 00	. 90
. 425		1. 00		. 75
. 450	1. 00	. 96	. 88	. 66
. 475				. 44
. 500	. 82	. 68	. 56	. 25
. 525				. 14
. 550		. 46	. 33	
. 600	. 58	. 30	. 16	
. 700	. 36	. 10		
. 800	. 20			
. 850	. 13			

TABLE IV

MEASURED LOCATIONS OF CIRCUMFERENTIAL NODE LINES—CYLINDER 2

(a) $m=2$

p, psig	$\frac{x_1}{L}$					
	$\frac{b}{L}=0$	$\frac{b}{L}=0.25$	$\frac{b}{L}=0.33$	$\frac{b}{L}=0.50$	$\frac{b}{L}=0.75$	$\frac{b}{L}=1.00$
0	----------	----------	----------	0. 339	----------	0. 580
. 5	----------	----------	0. 193	. 323	0. 442	. 545
1. 0	----------	0. 136	. 205	. 300	. 455	. 573
1. 5	----------	----------	----------	----------	. 432	----------
2. 0	----------	. 136	. 182	. 275	. 409	. 550
3. 0	----------	----------	----------	. 277	----------	----------
4. 0	----------	. 133	. 182	. 283	. 409	. 523
6. 0	----------	. 124	. 172	. 277	. 398	. 518
8. 0	0. 500	. 126	. 168	. 273	. 395	. 509

(b) $m=3$

p, psig	$\frac{x_1}{L}$	$\frac{x_2}{L}$	$\frac{x_1}{L}$	$\frac{x_2}{L}$	$\frac{x_1}{L}$	$\frac{x_2}{L}$	$\frac{x_1}{L}$	$\frac{x_2}{L}$	$\frac{x_1}{L}$	$\frac{x_2}{L}$	$\frac{x_1}{L}$	$\frac{x_2}{L}$
	$\frac{b}{L}=0$		$\frac{b}{L}=0.25$		$\frac{b}{L}=0.33$		$\frac{b}{L}=0.50$		$\frac{b}{L}=0.75$		$\frac{b}{L}=1.00$	
0	-----	-----	-----	-----	-----	-----	-----	-----	-----	-----	0. 482	0. 664
. 5	-----	-----	-----	-----	0. 136	0. 250	0. 173	0. 375	0. 300	0. 557	. 443	. 705
1. 0	-----	-----	0. 085	0. 159	. 132	. 245	. 195	. 368	. 290	. 568	. 409	. 672
2. 0	0. 331	0. 659	. 091	. 164	. 139	. 232	. 177	. 370	. 261	. 545	. 382	. 693
4. 0	-----	-----	. 088	. 173	. 125	. 223	. 182	. 345	. 261	. 523	. 341	. 673
6. 0	-----	-----	. 086	. 164	. 105	. 205	. 182	. 341	. 261	. 505	. 352	. 655
8. 0	. 381	. 670	. 079	. 159	. 125	. 216	. 182	. 340	. 261	. 500	. 354	. 670

COMPARISON OF THEORETICAL AND EXPERIMENTAL FREQUENCIES

EMPTY CYLINDERS

Unpressurized.—Theoretical and experimental variations of natural frequency with the number of circumferential waves n of cylinder 1, empty and unpressurized, are shown in figure 7. The theoretical frequencies for freely supported ends were calculated by use of equation (48). For fixed ends, equation (48) was used in conjunction with a correction procedure developed in reference 8. In reference 8, it is shown that the equations for freely supported ends can be used to predict fixed-end frequencies provided the axial wavelength factor $\lambda=\frac{m\pi a}{L}$ is replaced by an equivalent axial wavelength factor $\lambda_e=\frac{(m+0.3)\pi a}{L}$. It appears reasonable, therefore, to modify equation (48) in a similar manner to account for fixed ends.

A comparison of the frequencies calculated by equation (48) with those calculated by the method of reference 8 is presented in table VI in order to verify that equation (48) with the correction procedure of reference 8 may be used to predict frequencies of cylinders with fixed ends. The natural frequencies of cylinder 1 for several values of m and n are presented for freely supported ends in part (a) of table VI, and for fixed ends in part (b) of table VI. Table VI shows that the frequencies calculated by use of equation (48) are in close agreement with those calculated by the methods of reference 8 for both freely supported ends and for fixed ends. It can be concluded, therefore, that the equivalent wavelength factor λ_e can be used in equation (48) to calculate fixed-end frequencies.

TABLE V

MINIMUM NATURAL FREQUENCIES AS A FUNCTION OF WATER LEVEL

[Cylinder 2; $m = 1$]

b/L	Frequency f, cps, for $p =$:					
	0	0.5 psig	1.0 psig	2.0 psig	4.0 psig	8.0 psig
Major response below water level						
0	76	206	256	312	363	410
.063	----	204	255	302	354	400
.090	75	----	----	----	----	----
.100	----	195	227	256	300	340
.120	74	----	----	----	----	----
.125	----	165	193	216	236	258
.136	72	----	----	----	----	----
.157	67	----	----	----	----	----
.180	59	----	----	----	----	----
.200	----	110	124	138	148	----
.227	47	----	----	----	----	----
.250	----	90	104	117	127	140
.333	34	68	80	90	101	110
.500	30	47	53	62	69	77
.625	28	41	45	51	58	63
.750	27	38	41	46	52	58
.822	29	----	----	----	----	----
.910	30	----	----	----	----	----
1.00	30	36	39	42	47	51
Major response above water level						
0	----	206	256	312	363	410
.063	----	206	265	321	373	----
.125	----	210	280	333	390	440
.250	----	233	312	373	433	480
.333	----	253	342	403	470	518
.500	----	305	395	496	565	----
.625	----	380	473	576	----	----

The theoretical fixed-end frequencies shown in figure 7 were calculated by using the equivalent wavelength factor λ_e in equation (48). Figure 7 shows good overall agreement between the experimental frequencies, which were obtained with fixed ends, and the theoretical fixed-end frequencies. This figure also shows the unusual variation of frequency with n peculiar to cylindrical shells; that is, the lowest frequency does not occur with the simplest nodal pattern. In this case the lowest frequency occurs with $m = 1$ and $n = 10$. Comparison between the frequencies calculated for the freely supported cylinder and the fixed-end cylinder for a given value of m shows frequencies for the fixed-end configuration to be higher by as much as 28 percent in the minimum

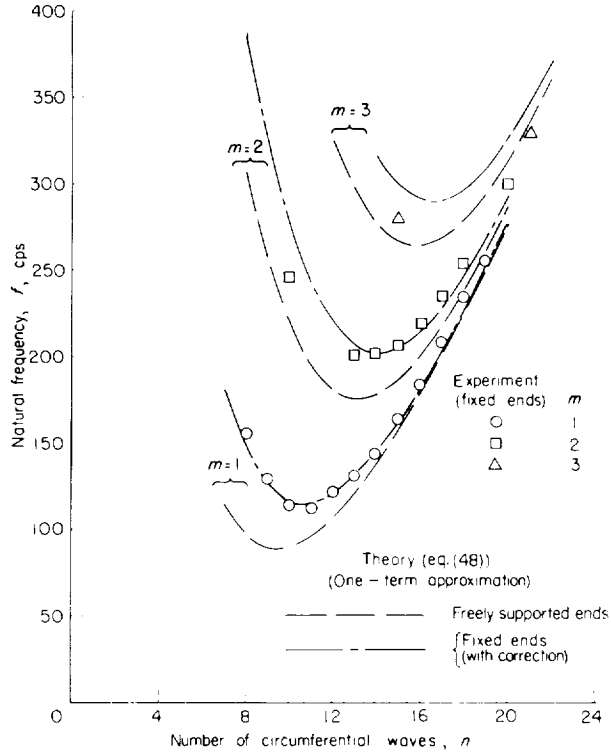

FIGURE 7.—Theoretical and experimental variation of natural frequency of an empty, unpressurized cylinder with the number of circumferential waves n. Cylinder 1; $a/h = 937$.

frequency area; however, small increases of n reduce this difference to less than 5 percent.

Pressurized.—Theoretical and experimental variations of the natural frequencies of cylinders 1 and 2 with the number of circumferential waves n are presented in figure 8 for internal pressures up to 8 psig. The theoretical frequencies shown in this figure were calculated from equation (48) with ends assumed to be freely supported since no theory is available for pressurized cylinders having fixed ends. The end conditions are expected to have only a small effect on frequencies for values of n above the n for minimum frequency. For values of n above the n for minimum frequency, the theoretical and experimental frequencies agree well, the theoretical frequencies being high by as much as 15 percent but usually high by less than 10 percent. The results in figure 8 indicate that, for values of n above n for minimum frequency, equation (48) adequately predicts the natural frequencies of empty, pressurized cylinders. This figure shows also that

TABLE VI

COMPARISON OF THE FREQUENCIES CALCULATED FOR CYLINDER 1 BY USE OF EQUATION (48) AND THE EQUATIONS OF REFERENCE 8

	Frequency f, cps, calculated by					
n	Eq. (48)	Ref. 8	Eq. (48)	Ref. 8	Eq. (48)	Ref. 8
	m 1		m 2		m 3	
(a) Freely supported ends; $\lambda=\frac{m\pi}{L}$						
7	115.02	115.01				
8	96.28	96.36	306.83	307.91		
9	88.47	88.55	254.38	255.67		
10	89.08	89.16	217.82	219.11		
11	95.90	96.05	193.84	195.06		
12	107.13	107.41	180.33	181.48	323.58	326.14
13			175.69	176.82	294.57	296.97
14	138.33	138.97	178.45	179.60	275.67	277.94
16	177.59	178.70	200.62	202.02	263.66	265.84
18	223.23	224.90	237.92	239.76	278.79	281.14
20	274.68	276.99	285.25	287.66	313.06	315.81
(b) Fixed ends; $\lambda=\frac{(m+0.3)\pi}{L}$						
7	182.27	182.40				
8	147.14	147.52	385.96	387.38		
9	126.10	126.52	320.76	322.45		
10	115.96	116.36	273.26	274.98		
11	114.56	114.96	239.73	241.37		
12	119.97	120.41	217.75	219.29	374.43	377.47
13			205.64	207.10	338.72	341.57
14	144.73	145.45	202.01	203.45	313.59	316.28
16	181.27	182.43	214.92	216.50	290.63	293.13
18	225.71	227.42	246.90	248.85	297.36	299.94
20	276.61	278.93	291.49	293.85	326.02	328.83

the internal pressure has a large effect on natural frequency; an increase of pressure from 1 psig to 8 psig results in a frequency increase for cylinder 2 from about 271 cps to about 712 cps at $n=10$.

PARTLY LIQUID-FILLED CYLINDERS

Theoretical and experimental variations of natural frequency with liquid depth are shown for $m=1$ and several values of n in figure 9 for cylinder 1 ($p=0$) and in figure 10 for cylinder 2 ($p=0.5$, 1, 2, 4, and 8 psig). Four theoretical curves are shown in these figures, all calculated on the assumption that the ends are freely supported. The first was calculated from equation (46), which was derived by using a single term of the displacement series, and the exact virtual mass expression (eqs. (31) and (32)); the second was calculated also from equation (46), but with the approximate virtual-mass expressions (eqs. (33) and (34)). The third curve was calculated from equation (51) with two terms of the displacement series and the approximate virtual-mass expressions; and the fourth curve, which is shown only in figure 9 for $n=18$, was calculated from equation (51) with two terms for the displacement series and the exact virtual-mass expressions.

Figures 9 and 10 show that all theoretical curves give the same frequencies for the empty condition, $b/L=0$, and for the nearly full condition, $b/L\approx 0.7$ to $b/L=1.0$. The theoretical and experimental frequencies are in close agreement in these ranges of b/L, except for some of the smaller values of n, where the disagreement can be attributed to the difference between the experimental and theoretical end conditions. The use of either expression for virtual mass in equation (46), which used a single-term displacement, yields results which agree fairly well with the experimental frequencies at small values of n, as shown by figures 9 and 10, but as n increases these theoretical frequencies become higher than the experimental frequencies in the range of b/L from about 0.1 to about 0.7. The reason for this result can be explained by comparison of the theoretical with the experimental mode shapes. For a one-term expansion the theoretical axial mode shape (eq. (43)) is symmetrical with respect to a point midway between the cylinder ends, but the experimental axial mode shape as shown by figure 4 is nonsymmetrical and the degree of nonsymmetry increases with increasing values of n. Thus, the higher theoretical frequencies are caused by the constraint of symmetry, which is not present in the physical system.

The use of two terms of the displacement series (eq. (50)) relaxes the symmetry constraint and results in lower theoretical frequencies as shown by the third theoretical curve in figures 9 and 10. This curve is shown to be in good agreement with the experimental data. In a few cases, for instance for some of the large values of n and small values of b/L, the curve given by equation (51) is slightly high, indicating that more relaxation of the symmetry constraint must be provided; that is, a third term must be included in the displacement series.

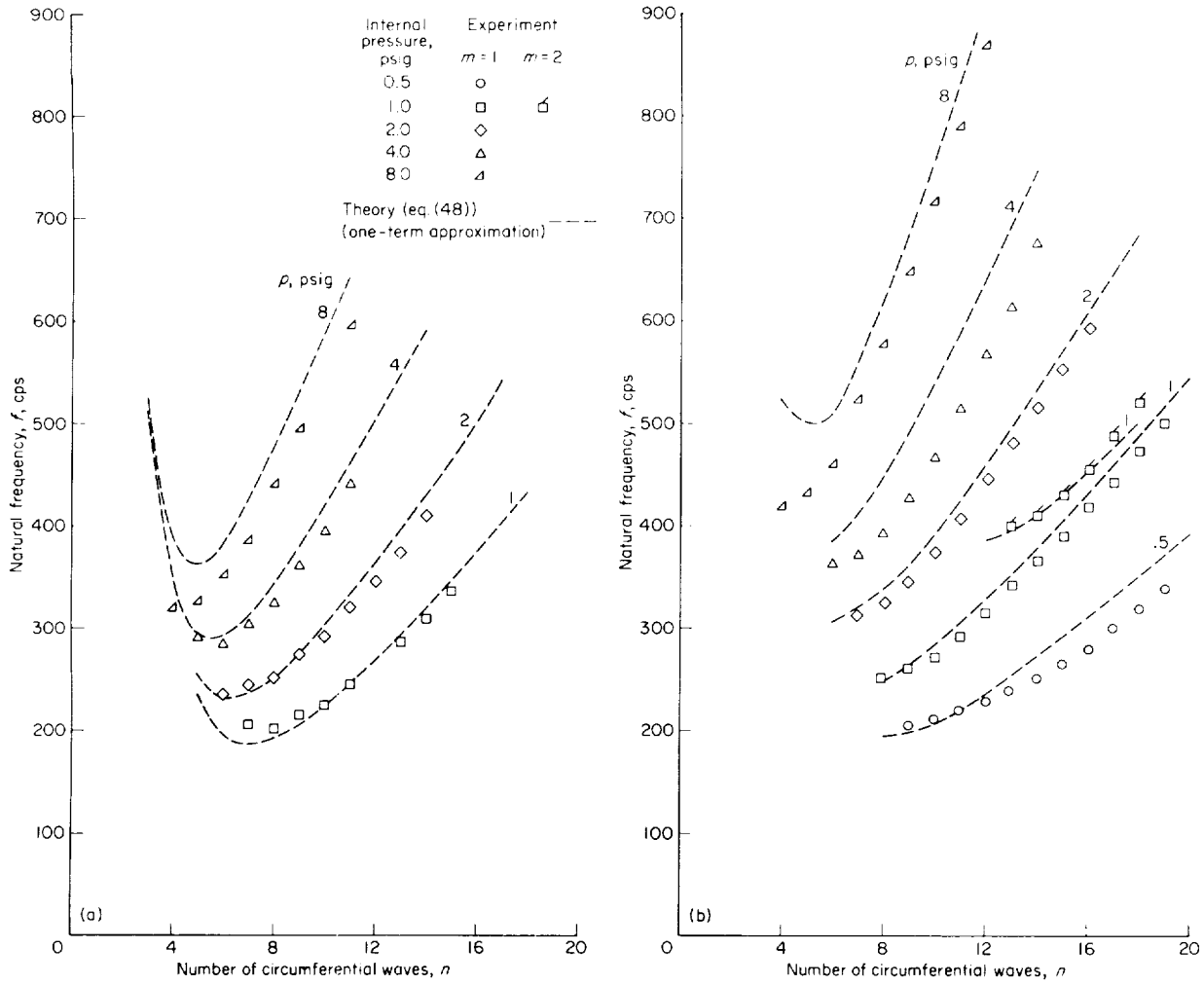

(a) Cylinder 1; $a/h = 937$.

(b) Cylinder 2; $a/h = 3{,}000$.

FIGURE 8.- Theoretical and experimental variation of natural frequency of empty, pressurized cylinders with the number of circumferential waves n. $b/L = 0$.

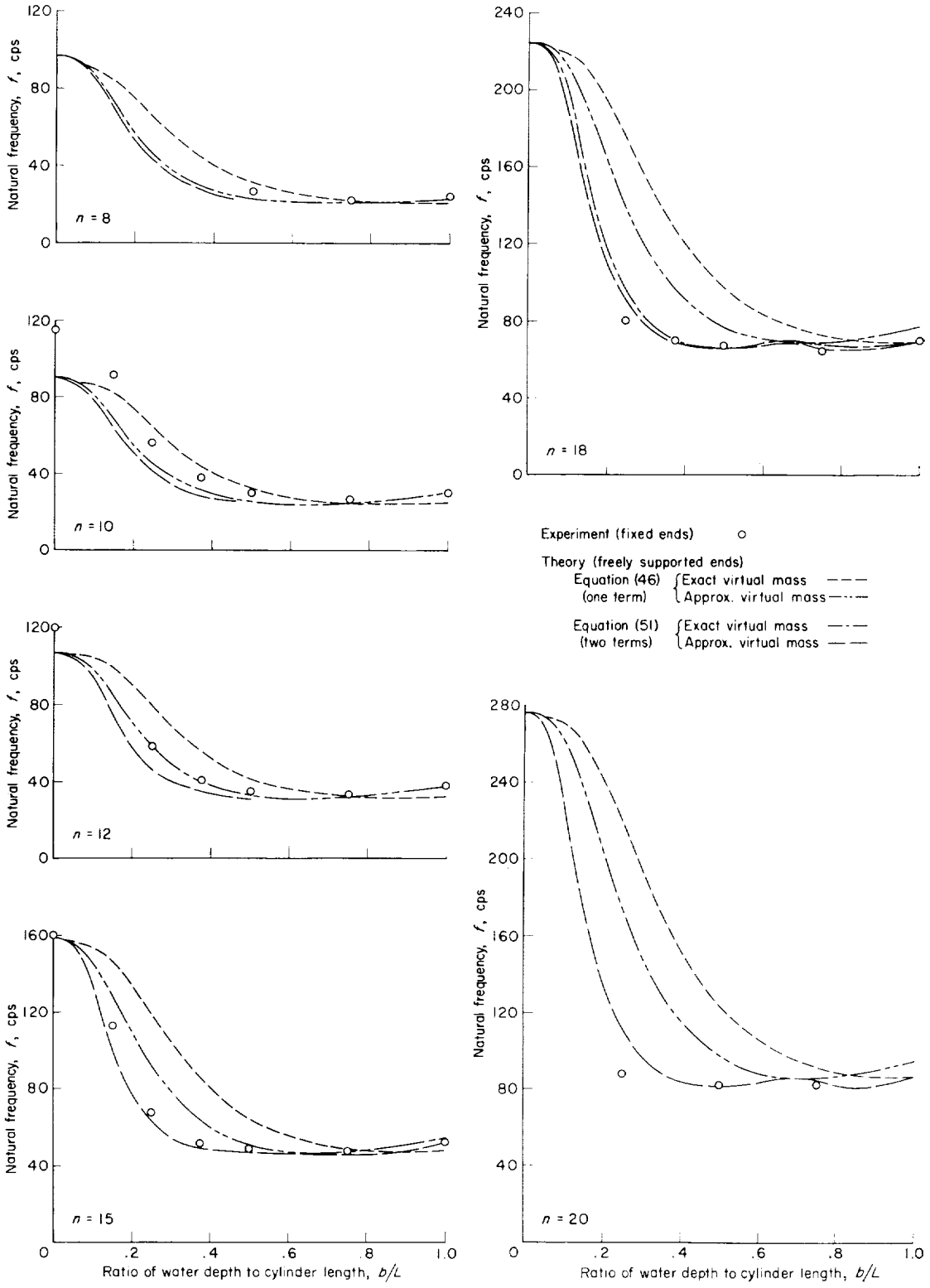

FIGURE 9.—Theoretical and experimental variation of natural frequency of an unpressurized cylinder with water depth. Cylinder 1; $m=1$.

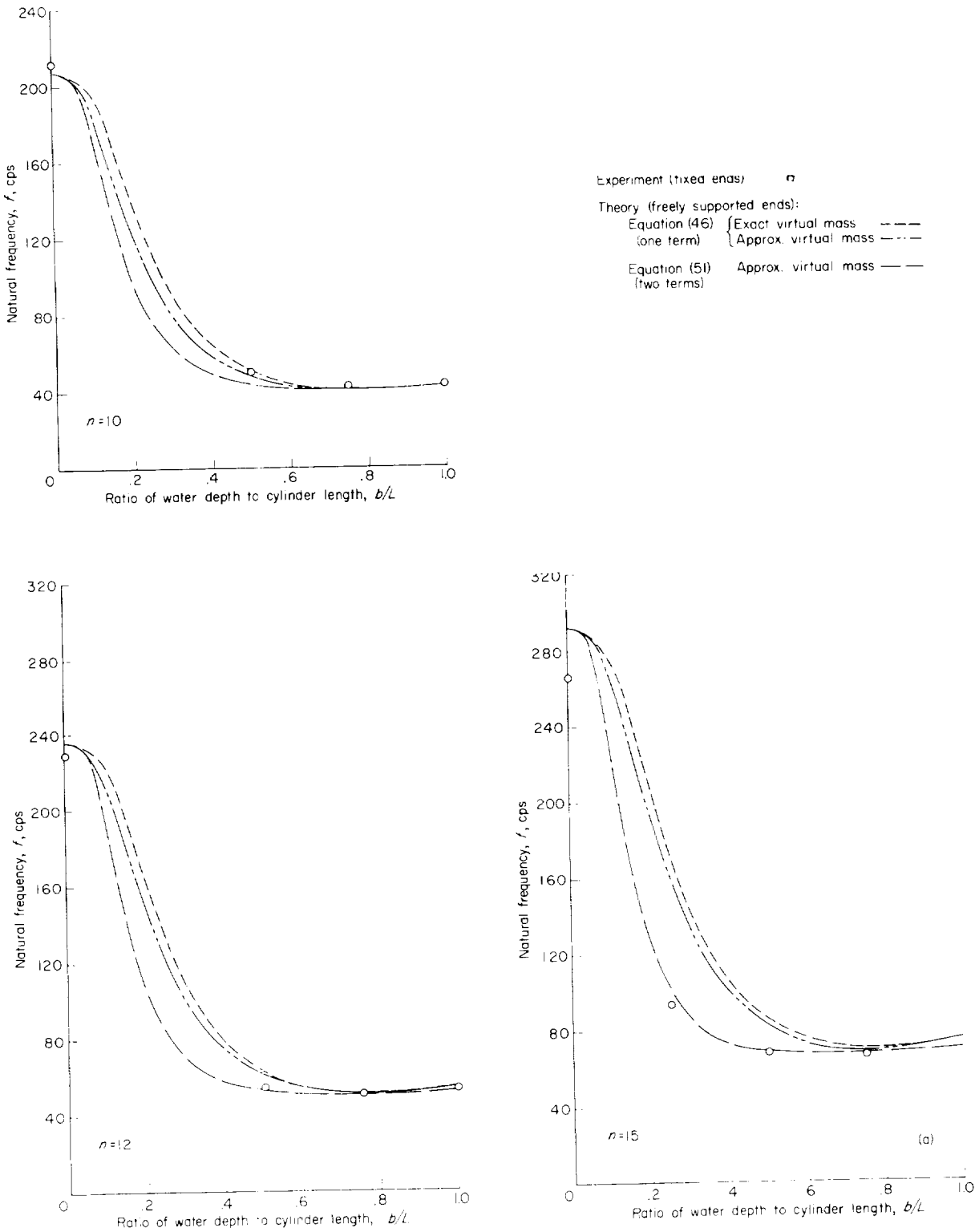

(a) $p=0.5$ psig.

FIGURE 10.—Theoretical and experimental variation of natural frequency of a pressurized cylinder with water depth. Cylinder 2; $m=1$.

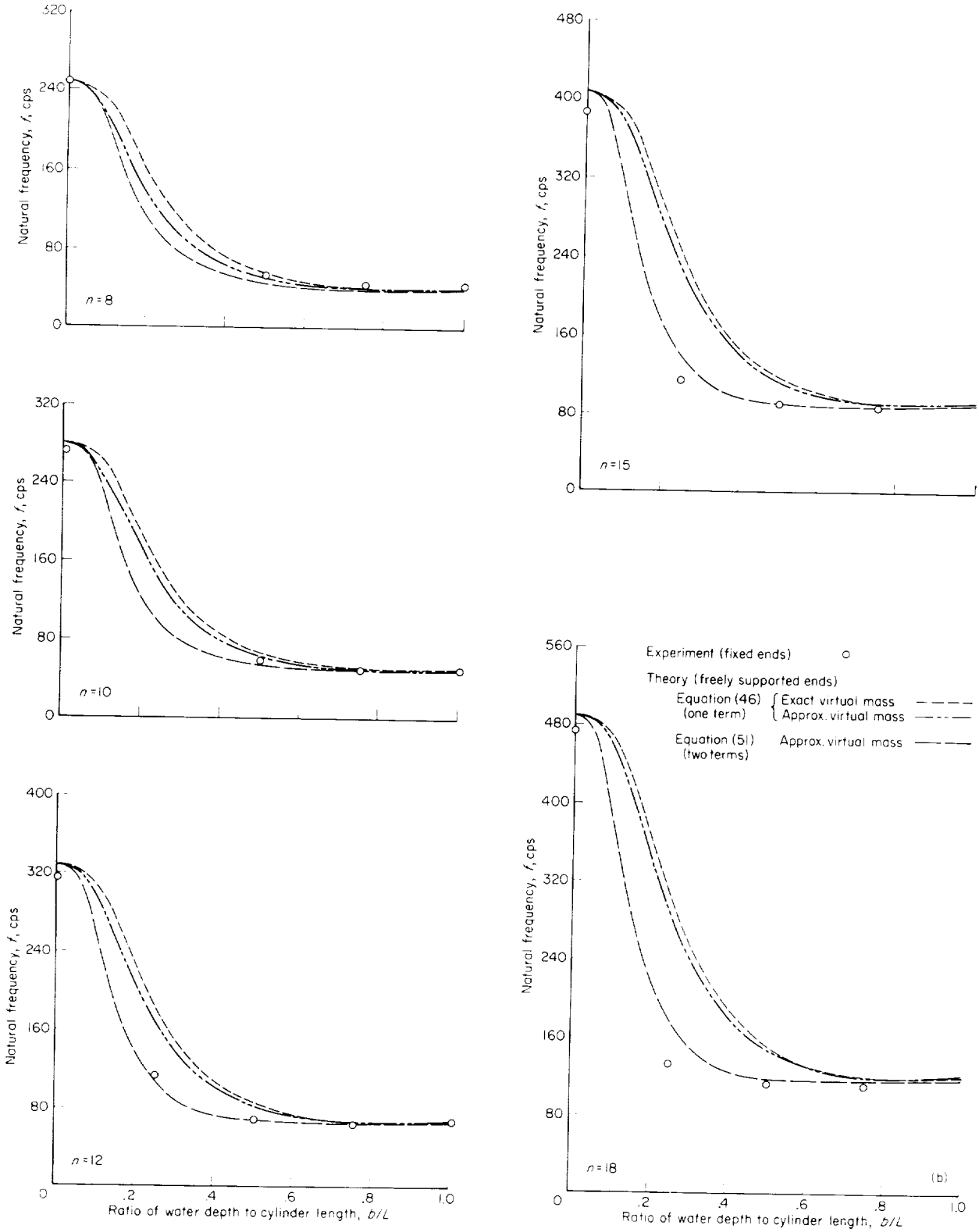

(b) $p=1.0$ psig.

FIGURE 10.—Continued.

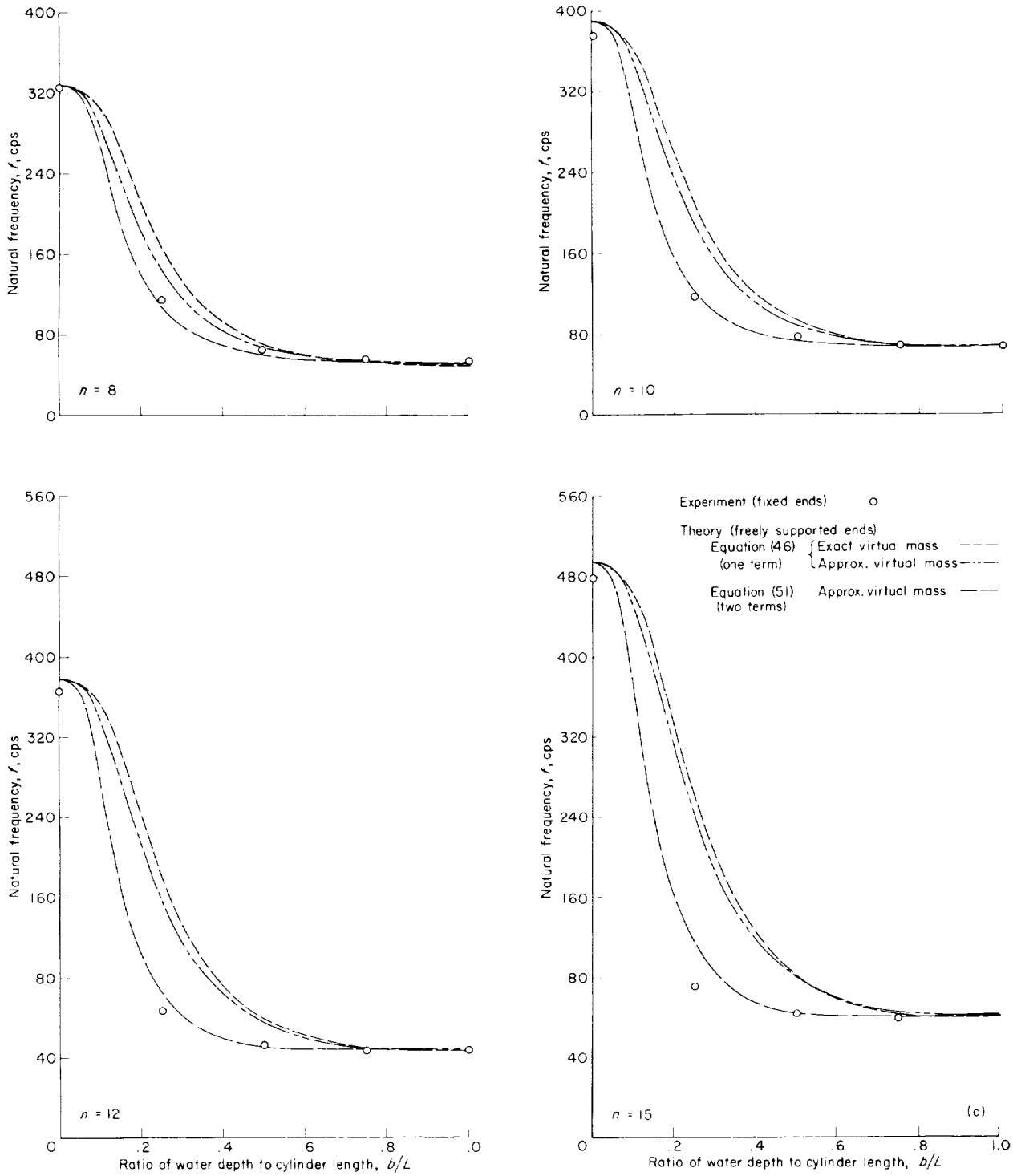

(c) $p=2.0$ psig.

FIGURE 10.—Continued.

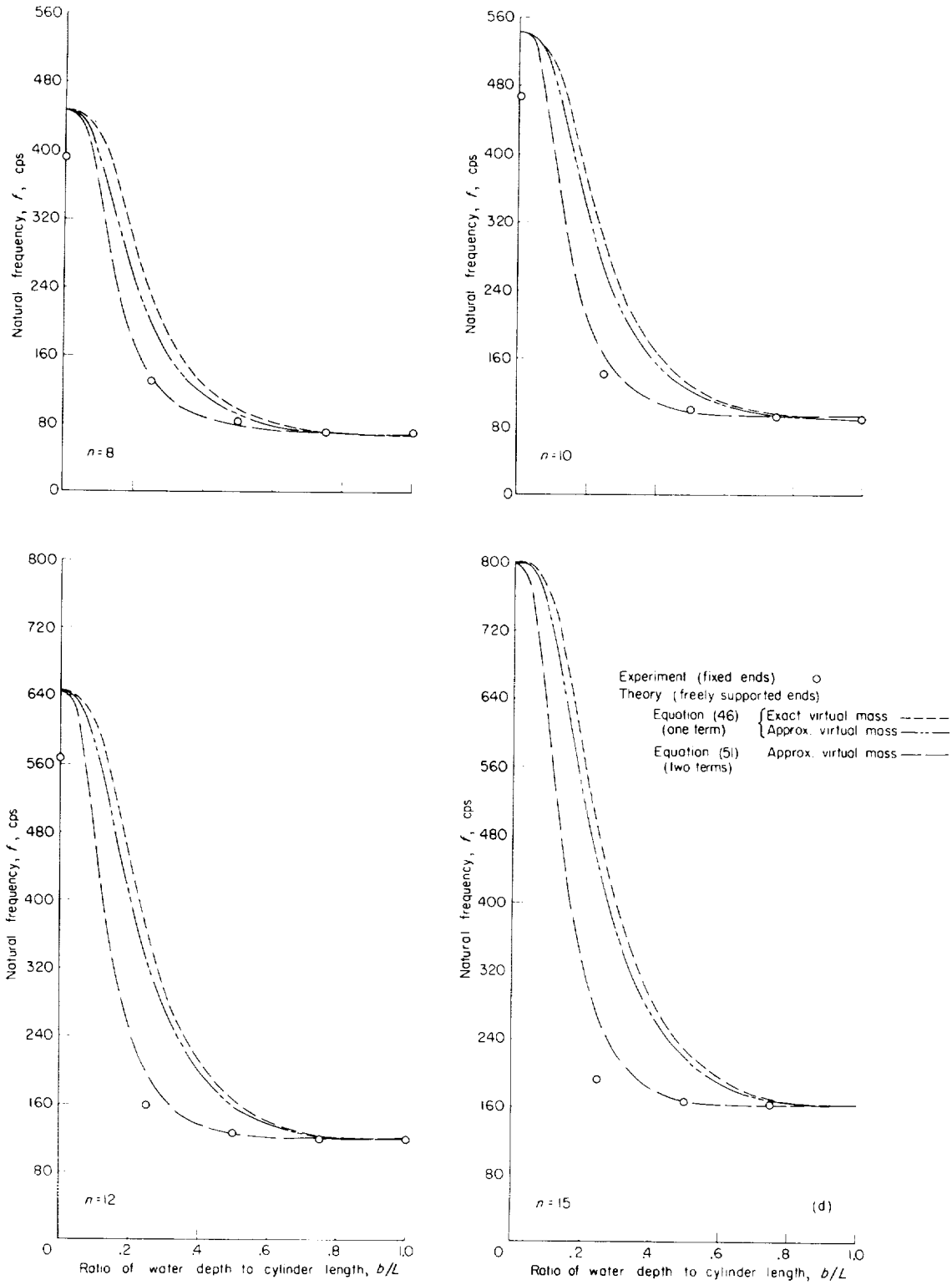

(d) $p = 4.0$ psig.

FIGURE 10.—Continued.

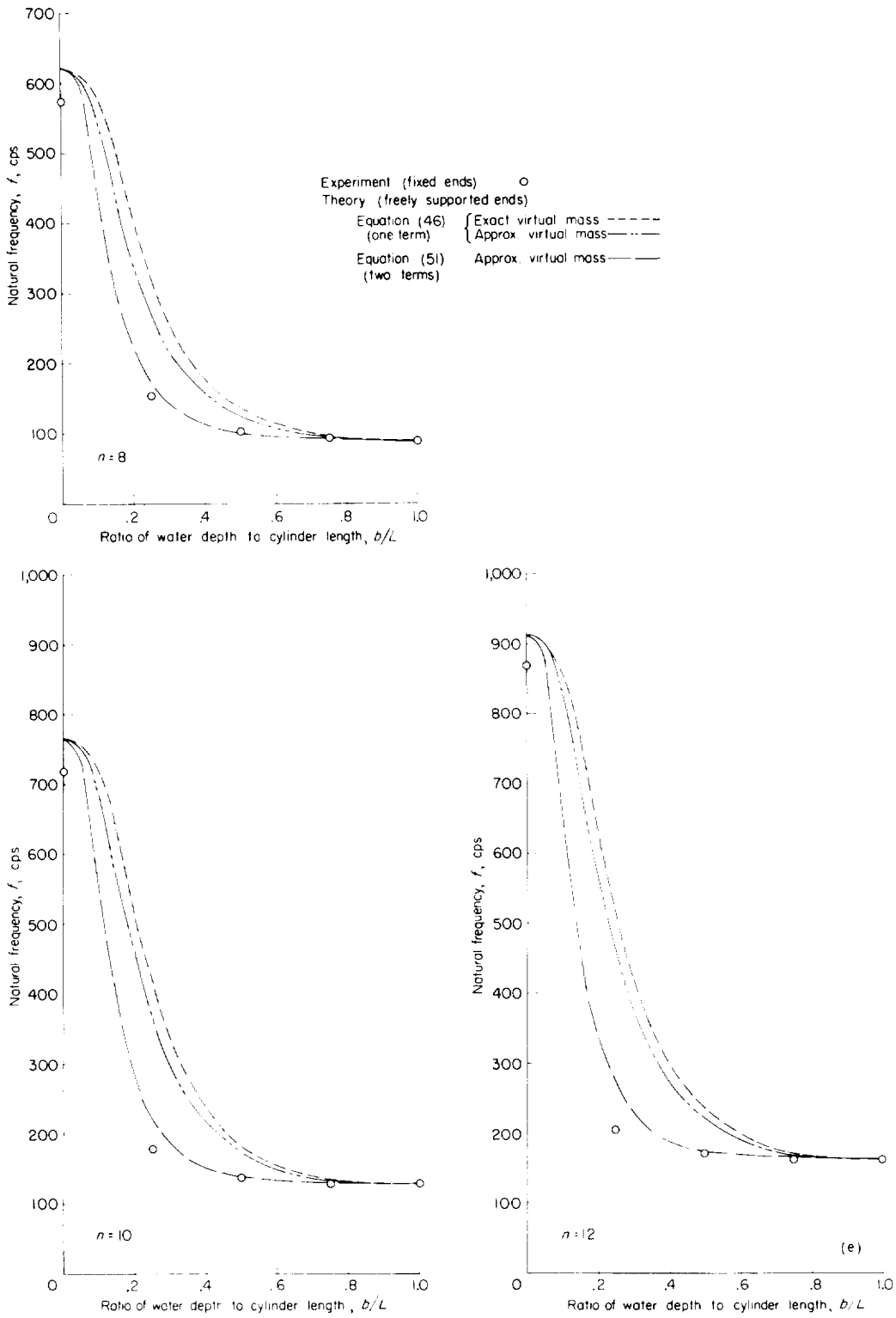

(e) $p = 8.0$ psig.

FIGURE 10.—Concluded.

The results shown in figures 9 and 10 indicate that equation (46) (the frequency equation for a one-term displacement) can be used to calculate frequencies for b/L from 0 to about 0.05 and from about 0.7 to 1.0. For the range of b/L from 0.05 to 0.70 equation (46) gives only a general idea of the variation of frequency with b/L; and if an accurate calculation of frequency is desired, the two-term representation of the displacement (eq. (51)) should be used. If even greater accuracy is desired, the general equation (eq. (40)) can be used to obtain a particular frequency equation for any desired number of terms of the displacement series. The results presented in figures 9 and 10 also show that the accuracy obtained by use of either the exact or approximate representation for virtual mass is essentially the same.

LIQUID-FILLED CYLINDERS

Theoretical and experimental variations of natural frequency with the number of circumferential waves n are shown in figure 11 for liquid-filled cylinders, one axial wave ($m=1$), and for several values of internal pressure. The theoretical curves in this figure were calculated from a one-term expansion (eq. (46)) and the approximate virtual mass expressions (eqs. (33) and (34)). This figure shows the theoretical and experimental frequencies to be in good agreement, from which it can be concluded that these equations predict adequately the frequencies of liquid-filled, pressurized cylinders.

CONCLUDING REMARKS

Results are reported of an investigation of the shell vibration characteristics of pressurized, thin-walled circular cylinders which are empty, partly filled, or full of liquid. This investigation consisted of a derivation of equations for calculation of natural frequencies of shell vibration and an experimental determination of natural frequencies, mode shapes, and damping of two thin-walled cylinders having radius-thickness ratios of 937 and 3,000.

The equations of motion for calculation of the natural frequency are derived by use of a Rayleigh-Lagrange procedure in which kinetic and potential energy expressions are developed in terms of the shell displacements. Shell displacement forms are then assumed, and the Lagrange equations are applied to yield a set of simultaneous equations from which natural frequencies are determined.

Comparisons of calculated and experimental frequencies show that the equations derived are adequate for the prediction of the natural frequencies of the cylinder. For partly filled cylinders the results show that it is necessary to use more than one term of the assumed displacement series; a two-term series is shown to give good agreement with the experimental data of the present investigation. When the liquid depth is zero, the equations reduce to a single, relatively simple equation for frequency which has been derived previously by Eric Reissner. It is shown that this equation may be used for calculation of frequencies of empty, pressurized or unpressurized cylinders with either fixed or freely supported ends. When the cylinders are filled with liquid, a single term of the displacement series is shown to give frequencies which agree well with the experimental frequencies.

LANGLEY RESEARCH CENTER,
NATIONAL AERONAUTICS AND SPACE ADMINISTRATION,
LANGLEY STATION, HAMPTON, VA., *February 23, 1962*

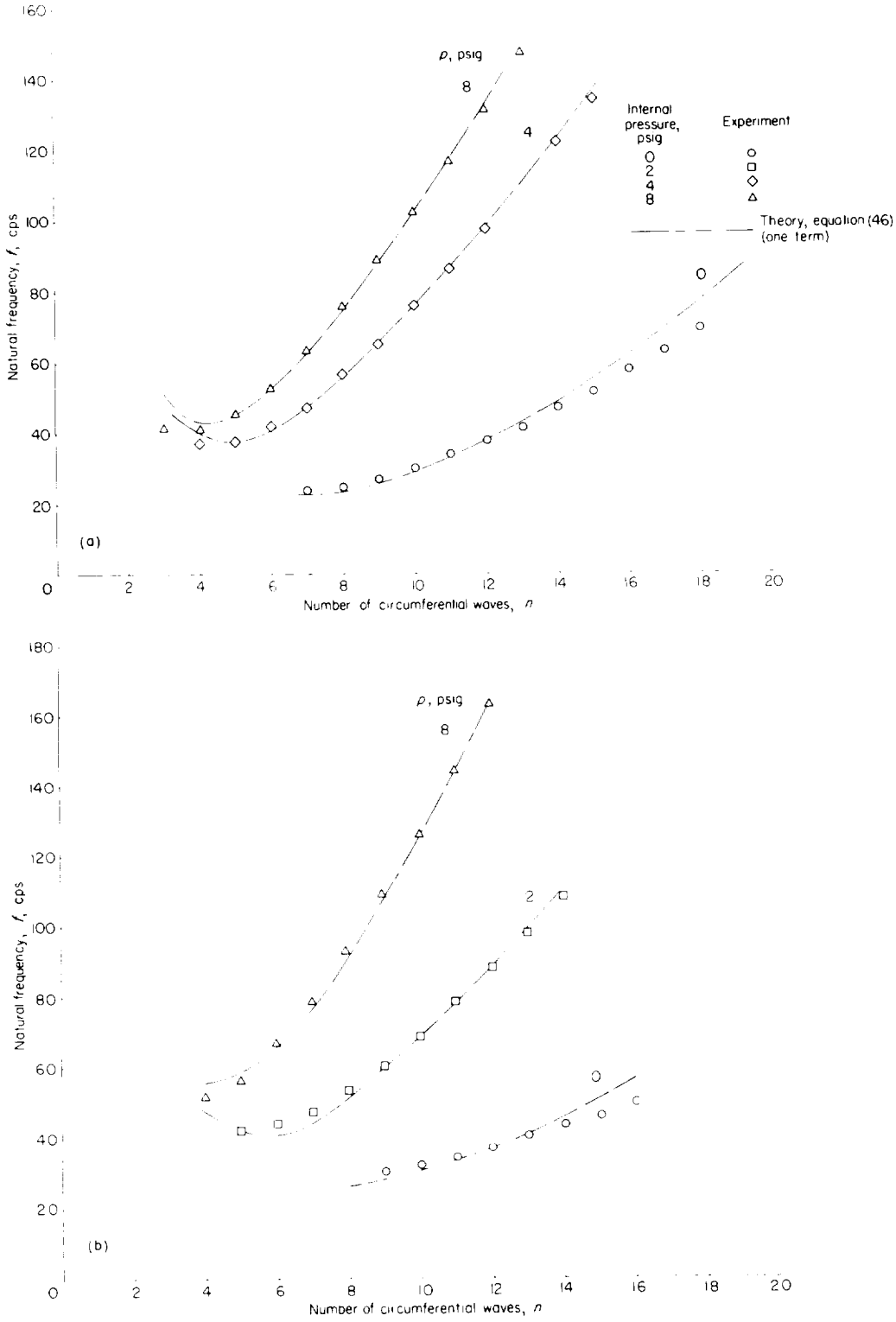

(a) Cylinder 1; $a/h = 937$.
(b) Cylinder 2; $a/h = 3{,}000$.

FIGURE 11.—Theoretical and experimental variation of natural frequency of pressurized, water-filled cylinders with the number of circumferential waves n. $m = 1$.

APPENDIX

APPROXIMATE VIRTUAL MASS COEFFICIENTS

Approximate expressions for the virtual-mass coefficients of the partly filled cylinder, $m_{v1}(s)$, $m_{v2}(s,k)$, are obtained by use of a virtual-mass expression which was derived in reference 5 for liquid-filled cylinders. Equations were derived in reference 5 for the calculation of the natural frequencies of vibration of a thin-walled cylinder full of inviscid, compressible fluid. It is shown therein that the effects of the fluid on the shell vibration frequencies can be described by adding an equivalent fluid mass per unit area to the mass of the shell. When the fluid is incompressible, the equivalent fluid mass m_v is given by the expression

$$m_v=\frac{\rho_l a}{g} f_n(\lambda_0) \tag{A1}$$

For the partly filled cylinder it is assumed that an equivalent fluid mass per unit area, given by equation (A1), is distributed over the wetted area of the shell and is moving radially with the shell. With this assumption the kinetic energy of the fluid can be obtained from the expression

$$T_l=\int_0^{2\pi}\int_0^b \frac{1}{2} m_v \dot{w}^2 a\,dx\,d\varphi \tag{A2}$$

where T_l is the kinetic energy of the fluid, and the radial velocity $\dot{w}$ is obtained from the radial displacement w

$$w=\cos n\varphi \sum_{s=0}^{N} W_s(t) \sin \frac{\lambda_s x}{a} \tag{A3}$$

With the substitution of the fluid mass (eq. (A1)) and the radial velocity from equation (A3) into equation (A2), the following expression for the kinetic energy can be obtained:

$$T_l=\frac{\rho_l a^2}{2g}\sum_{s=0}^{N} f_n(\lambda_0)\dot{W}_s(t)^2\int_0^{2\pi}\int_0^b \cos^2 n\varphi \sin^2 \frac{\lambda_s x}{a}\,dx\,d\varphi$$

$$+\frac{\rho_l a^2}{2g}\sum_{s=0}^{N}\sum_{\substack{k=0\\k\neq s}}^{N} f_n(\lambda_0)\dot{W}_s(t)\dot{W}_k(t)\int_0^{2\pi}\int_0^b \cos^2 n\varphi \sin \frac{\lambda_s x}{a}\sin \frac{\lambda_k x}{a}\,dx\,d\varphi \tag{A4}$$

Upon evaluation of the integrals in equation (A4) the kinetic energy of the fluid may be written as

$$T_l=\frac{\pi\rho_l a^2 b}{4g}\sum_{s=0}^{N}\left[m_{v1}(s)\dot{W}_s(t)^2 + \sum_{\substack{k=0\\k\neq s}}^{N} m_{v2}(s,k)\dot{W}_s(t)\dot{W}_k(t)\right] \tag{A5}$$

where the virtual mass coefficients, $m_{v1}(s)$ and $m_{v2}(s,k)$ are:

$$m_{v1}(s)=f_n(\lambda_0)\left(1-\frac{\sin\frac{2\lambda_s b}{a}}{\frac{2\lambda_s b}{a}}\right) \tag{A6}$$

$$m_{v2}(s,k)=f_n(\lambda_0)\left[\frac{\sin(\lambda_s-\lambda_k)\frac{b}{a}}{(\lambda_s-\lambda_k)\frac{b}{a}}-\frac{\sin(\lambda_s+\lambda_k)\frac{b}{a}}{(\lambda_s+\lambda_k)\frac{b}{a}}\right] \tag{A7}$$

Comparison shows that the virtual mass coefficients given by equations (A6) and (A7) are similar, respectively, to the first terms of the so-called exact virtual mass coefficients given by equations (31) and (32). The only difference is the appearance of the term $f_n(\lambda_0)$ in equations (A6) and (A7) in place of the term $f_n(\lambda_s)$ in the exact expression. This suggests that the first terms of equations (31) and (32) be used as an approximation to the virtual mass coefficients. The approximate virtual mass coefficients thus arrived at are

$$m_{v1}(s)=f_n(\lambda_s)\left[1-\frac{\sin\frac{2\lambda_s b}{a}}{\frac{2\lambda_s b}{a}}\right] \tag{A8}$$

and

$$m_{v2}(s,k)=f_n(\lambda_s)\left[\frac{\sin(\lambda_s-\lambda_k)\frac{b}{a}}{(\lambda_s-\lambda_k)\frac{b}{a}}-\frac{\sin(\lambda_s+\lambda_k)\frac{b}{a}}{(\lambda_s+\lambda_k)\frac{b}{a}}\right] \tag{A9}$$

REFERENCES

1. Rayleigh (Lord): The Theory of Sound. First Am. ed., vol. I, Dover Pub., 1945, pp. 395–432.
2. Love, A. E. H.: A Treatise on the Mathematical Theory of Elasticity. Fourth ed. (First Am. Printing), Dover Pub., 1944.
3. Baron, M. L., and Bleich, H. H.: Tables for Frequencies and Modes of Free Vibration of Infinitely Long Thin Cylindrical Shells. Jour. Appl. Mech., vol. 21, no. 2, June 1954, pp. 178–184.
4. Reissner, Eric: Non-Linear Effects in Vibrations of Cylindrical Shells. Rep. No. AM 5–6, Guided Missile Res. Div., The Ramo-Wooldridge Corp., Sept. 30, 1955.
5. Berry, J. G., and Reissner, E.: The Effect of an Internal Compressible Fluid Column on the Breathing Vibrations of a Thin Pressurized Cylindrical Shell. Jour. Aero. Sci., vol. 25, no. 5, May 1958, pp. 288–294.
6. Baron, Melvin L., and Bleich, Hans H.: The Dynamic Analysis of Empty and Partially Full Cylindrical Tanks. Part I—Frequencies and Modes of Free Vibration and Transient Response by Mode Analysis. DASA No. 1123A (Contract DA–29–044–XZ–557), Defense Atomic Support Agency, May 1959. (Available from ASTIA.)
7. Arnold, R. N., and Warburton, G. B.: Flexural Vibrations of the Walls of Thin Cylindrical Shells Having Freely Supported Ends. Proc. Roy. Soc. (London), ser. A, vol. 197, no. 1049, June 7, 1949, pp. 238–256.
8. Arnold, R. N., and Warburton, G. B.: The Flexural Vibrations of Thin Cylinders. Proc. (A) Inst. Mech. Eng. (London), vol. 167, no. 1, 1953, pp. 62–74.
9. Fung, Y. C., Sechler, E. E., and Kaplan, A.: On the Vibration of Thin Cylindrical Shells Under Internal Pressures. Jour. Aero. Sci., vol. 24, no. 9, Sept. 1957, pp. 650–660.
10. Reissner, Eric: On Vibrations of Shallow Spherical Shells. Jour. Appl. Phys., vol. 17, no. 12, Dec. 1946, pp. 1038–1042.
11. Lamb, Horace: Hydrodynamics. Sixth ed., Dover Pub., 1945.
12. Herr, Robert W.: A Wide-Frequency-Range Air-Jet Shaker. NACA TN 4060, 1957.

U.S. GOVERNMENT PRINTING OFFICE: 1963